Economic Geology, v. 109, pp. 1563–1583

Geochemistry Insights on the Genesis of the Subduction-Related Heishan Magmatic Ni-Cu-(PGE) Deposit, Gansu, Northwestern China, at the Southern Margin of the Central Asian Orogenic Belt*

Wei Xie,[1] Xie-Yan Song,[1,†] Lie-Meng Chen,[1] Yu-Feng Deng,[1] Wen-Qin Zheng,[1] Yu-Shan Wang,[2] Duo-Heng Ba,[2] Mao-Hong Yin,[2] and Yan Luan[1]

[1] *State Key Laboratory of Ore Deposit Geochemistry, Institute of Geochemistry, Chinese Academy of Sciences, 46th Guanshui Road, Guiyang, 550002, P. R. China*

[2] *Jinchuan Group Ltd, Jinchang, Gansu, 737100, P. R. China*

Abstract

The Devonian subduction-related Heishan mafic-ultramafic intrusion hosting a magmatic Ni-Cu-(PGE) deposit is situated at the southern margin of the Central Asian orogenic belt. The outcrop of the intrusion is ~800 m long and ~470 m wide and dips to the southwest to depths up to 1,300 m. The Heishan intrusion is emplaced in Neoproterozoic dolomitic marble and siliceous slate and dominantly comprises of harzburgite and lherzolite. The stratigraphic reversals of Fo and Ni contents of olivine within the lerzolite and harzburgite indicate injections of several pulses of magmas. The two orebodies (Nos. 1 and 4) within the harzburgite and lherzolite at the lower part of the intrusion host ~35 million metric tons (Mt) of disseminated sulfide mineralization with average grades of 0.6 wt % Ni and 0.3 wt % Cu. The sulfides of the No. 4 orebody are lower in PGE contents on the basis of 100% sulfide (580-1,860 ppb Pt, 720-1,450 ppb Pd, 50-120 ppb Ir) and higher in Cu/Pd ratios (48,000-75,000) relative to the sulfides of the No. 1 orebody and mineralized harzburgites, which have 2,350 to 4,110 ppb Pt, 3,460 to 5,840 ppb Pd, 130 to 160 ppb Ir and Cu/Pd ratios of 16,000 to 26,000. Additionally, the olivines in the No. 1 orebody and mineralized harzburgites have higher forsterite (Fo) and Ni contents than those in the No. 4 orebody. We propose that the sulfide segregation of the No. 4 orebody was associated with extensive introduction of crustal sulfur, which is indicated by high $\delta^{34}S$ values (1.9–6.1‰) and low Se/S ratios (230–390 × 10^{-6}). Reworking of early fractionated massive or net-textured sulfides by the new wave of magma containing unfractionated sulfide droplets resulted in the positive correlation between Pd/Ir and Ni/Ir for the disseminated sulfides of the No. 4 orebody. In contrast, low $\delta^{34}S$ values (0.43–1.01‰) and restricted range of Pd/Ir ratios indicate that the high PGE contents of the sulfides in the No. 1 orebody and mineralized harzburgites resulted from reaction between the sulfides and new pulses of S-undersaturated magmas. The low PGE grades of the Heishan sulfides indicate that the sulfides were segregated from PGE-depleted parental magmas.

Introduction

Most world-class magmatic sulfide deposits are genetically linked with mantle plumes with magmatism close to craton margins. Examples include Noril'sk, Jinchuan, and Voisey's Bay (e.g., Naldrett, 2004, 2010; Song et al., 2006, 2009b, 2012; Begg et al., 2010; Maier and Groves, 2011; Chen et al., 2013). Notwithstanding, economic Ni-Cu sulfide deposits and potentially economic sulfide mineralization have been also discovered in orogenic belts in the past decades, such as the Aguablanca deposit in southwestern Spain (Casquet et al., 2001; Piña et al., 2006), the Tati and Selebi-Phikwe deposits in Botswanna (Maier et al., 2008), and the Duke Island sulfide mineralization in Alaska (Thakurta et al., 2008). These discoveries indicate the potential of orogenic belts to host magmatic sulfide deposits. The mechanisms of the sulfide segregation and emplacement in these Ni-Cu-(PGE) sulfides are not fully understood.

At the southern margin of the Central Asian orogenic belt, northwestern China, a number of 0.03- to ~5-km^2 variable-sized intrusions host mineralization with a total contained metal content of >1.5 million metric tons (Mt) of Ni and >1.2 Mt of Cu (Fig. 1, Zhou et al., 2004; Song and Li, 2009; Qin et al., 2011; Song et al., 2011; Xie et al., 2011; Gao et al., 2012, 2013; Sun et al., 2013; Xia et al., 2013; Deng et al., 2014 and references therein). Most of the sulfide mineralization is hosted by Permian-aged mafic-ultramafic intrusions, such as Kalatonge, Huangshandong, Huangshan, Pobei, Baishiquan, and Tianyu (270–290 Ma), and these intrusions have been linked to magmas derived from melting of the metasomatized mantle due to upwelling of asthenosphere in syn- or postsubduction environment (e.g., Han et al., 2004; Zhang et al., 2009; Song et al., 2011; Tang et al., 2011; Li et al., 2012). Only a few Ni-Cu sulfide mineralized intrusions, such as Jingbulake (431 ± 6 Ma) and the Tulargen No. 2 and No. 3 intrusions (358 ± 3 and 351 ± 4 Ma), were confirmed to be related to early subduction magmatism (Yang and Zhou, 2009; San et al., 2010). Widespread volcanics and intrusions (349–~330 Ma) at the southern margins of the Central Asian orogenic belt (Fig. 1) were proposed to be subduction related (Wang and Xu, 2006; Zhou et al., 2010).

As shown in Figure 1, the Heishan mafic-untramafic intrusion is situated in the eastern Beishan fold belt at the southern margin of the Central Asian orogenic belt and contains ~35 Mt of disseminated sulfide mineralization with average grades of 0.6 wt % Ni and 0.3 wt % Cu. Zircon U-Pb ages (~357 Ma) and trace element and radiogenic-isotope geochemistry indicate that the magma of the Heishan intrusion originated by partial melting of a mantle wedge triggered by

† Corresponding author: e-mail, songxieyan@vip.gyig.ac.cn

*A digital supplement to this paper is available at http://economicgeology.org/ and at http://econgeol.geoscienceworld.org/.

Submitted: March 2, 2013
Accepted: November 24, 2013

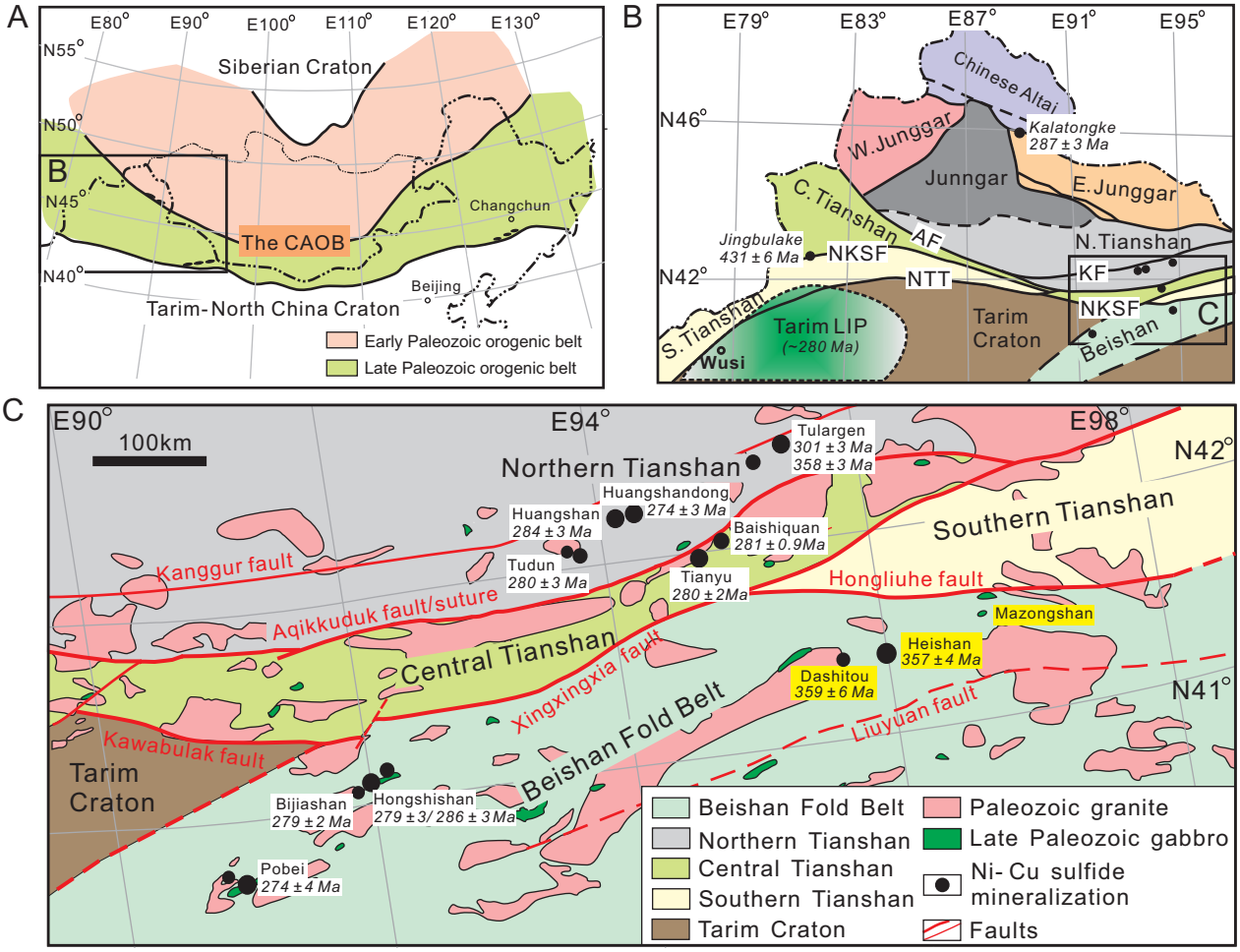

FIG. 1. A. Schematic geologic map of the Central Asian orogenic belt (CAOB). B. Tectonic units of northern Xinjiang, northwestern China (AF = Aqikkuduk fault, KF = Kanggur fault, NKSF = Nalati-Kawabulak-Xingxingxia fault, NTT = North Tarim thrust). C. Simplified geologic map of the Beishan fold belt (after BGMRG, 1989 and BGMRXUAR, 1993). The ages of the intrusions are from Han et al. (2004), San et al. (2010), Qin et al. (2011), Xie et al. (2012), Song et al. (2013, and references therein).

upwelling of asthenosphere due to slab break-off in the Late Devonian at an active continental margin (Xie et al., 2012). We use the Heishan deposit as an example to help to understand the features of the magmatic sulfide mineralization produced before collision at the southern margin of the Central Asian orogenic belt. In this paper, we report data for the chalcophile elements (Ni, Cu, as well as platinum-group elements), semimetal elements (Se, As, Te, and Bi), and S isotopes of the Heishan intrusion to constrain the genesis of a magmatic sulfide deposit at an active continental margin.

Geologic Background

The Central Asian orogenic belt extends >5,000 km west to east and is a complex collage of continental fragments, island arc assemblages, remnants of oceanic crust, and continental margins between the Siberian craton to the north and the Tarim-North China craton to the south (Fig. 1A). The Central Asian orogenic belt was formed by multiple subduction-accretion and collision processes from the Neoproterozoic to the Late Paleozoic (Sengör et al., 1993; Jahn et al., 2004; Xiao et al., 2004, 2008, 2010; Windley et al., 2007). The southern Central Asian orogenic belt in northwestern China consists, from north to the south, of the Chinese Altai, Junggar, Tianshan, and Beishan domains (Fig. 1B, Song et al., 2011). The Tianshan domain is subdivided by the Aqikkuduk and Nalati-Kawabulak-Xingxingxia faults into Northern, Central, and Southern Tianshan terranes, respectively (Fig. 1B; e.g., Xiao et al., 2004; Han et al., 2011; Ge et al., 2012).

The Early Permian magmatic sulfide mineralization occurs at the northern margin of the Junggar terrane (Kalatongke), in the Central Tianshan terrane (e.g., Tianyu), the Beishan fold belt (e.g., Pobei), and the Northern Tianshan terrane (e.g., Huangshan, Huangshandong, Tudun; Fig. 1, Mao et al., 2008; Qin et al., 2011; Song et al., 2011, 2013; Gao et al., 2012, 2013; Sun et al., 2013; Xia et al., 2013; Deng et al., 2014, and references therein). A few Ni-Cu sulfide mineralized intrusions, such as the Carboniferous Tulargen intrusion (No. 1 intrusion 301 ± 3 Ma; No. 2 intrusion 358 ± 3 Ma; No. 3 intrusion 351 ± 4 Ma, San et al., 2010, Jiao et al., 2013) and the Silurian Jingbulake Alaska-type intrusion (431 ± 6 Ma, Yang and Zhou, 2009) are located in the Northern and Central Tianshan terranes, respectively (Fig. 1B, C).

The NEE-SWW-trending Beishan fold belt is located to the northeast of the Tarim block at the southernmost margin of the Central Asian orogenic belt (Fig. 1). It is separated from the Tianshan terranes to the northwest by the Xingxingxia and Hongliuhe faults (Fig. 1C, BGMRG, 1989; BGMRXUAR, 1993; Xie et al., 2012). The Devonian Heishan Ni-Cu-(PGE) sulfide deposit is located at the eastern part of the Beishan fold belt, and the Early Permian Ni-Cu-(PGE) sulfide-mineralized Pobei and Hongshishan intrusions are situated in the western portion of the fold belt (Fig. 1C, Song et al., 2011).

Geology of the Heishan Deposit

The oval-shaped Heishan mafic-ultramafic intrusion has a length of ~800 m, a width of ~470 m, and a thickness of ~400 m, and dips to the southwest to depths up to 1,300 m (Fig. 2). It cuts the Neoproterozoic dolomitic marble and

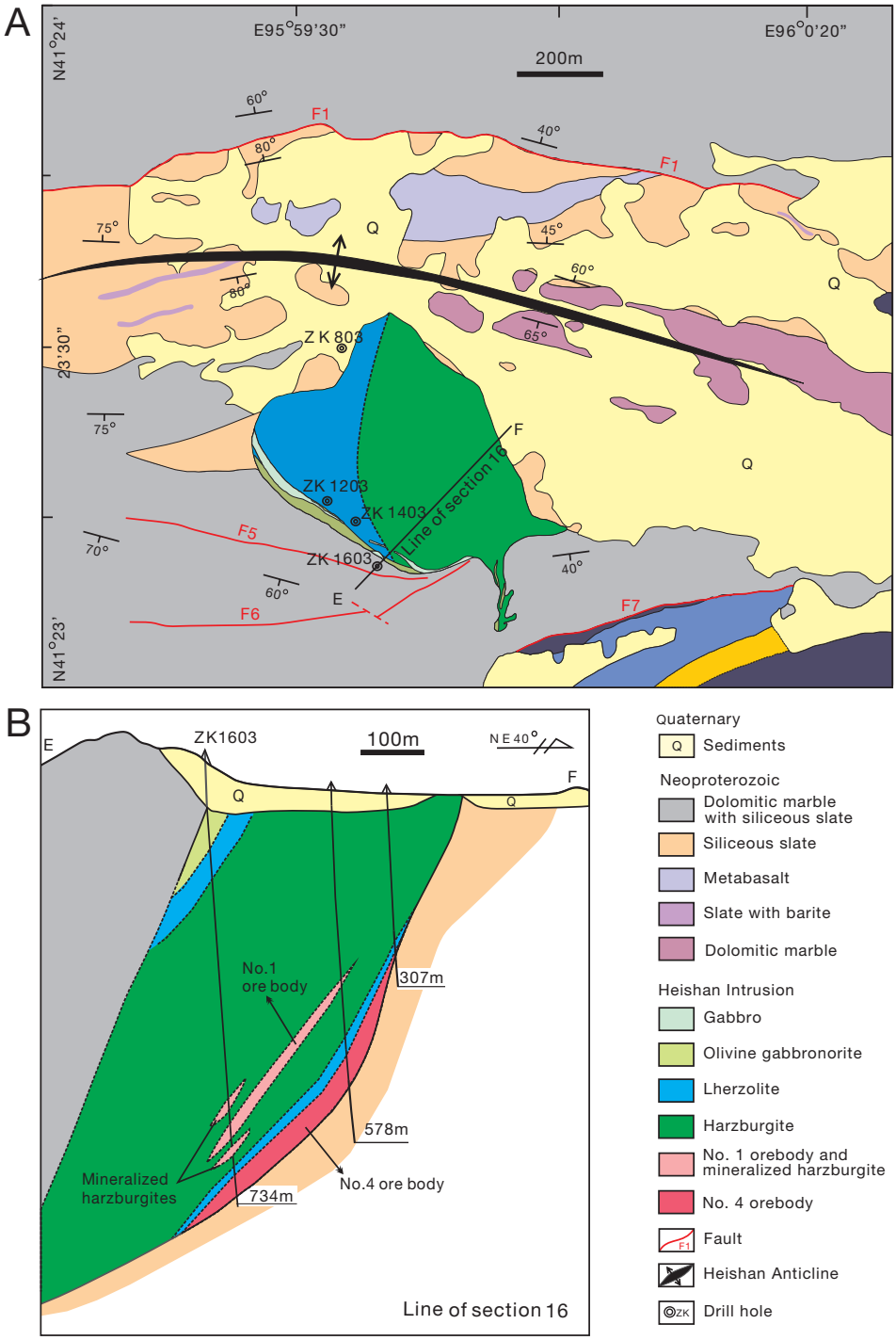

FIG. 2. (A). Simplified geologic map of the Heishan intrusion. (B). Cross section of the prospecting line 16, showing the lithologic and sulfide mineralization units (after Wei Xie, unpub. Ph.D. thesis).

siliceous slate with interlayers of metabasalt and andesite. Pyrite and other sulfides are absent in the country rocks. The Heishan intrusion is dominantly composed of harzburgite and lherzolite (Fig. 2). According to the petrologic observations by Xie et al. (2012), the harzburgite comprises 40 to 75 modal % olivine (Ol), 15 to 40% orthopyroxene (Opx), <10% plagioclase (Pl), and minor hornblende (Hbl) and biotite (Bt). With decreasing Ol and Opx upward, the harzburgite grades into lherzolite, which consists of 35 to 60% Ol, 20 to 30% Opx, 10 to 25% Cpx (clinopyroxene), 5 to 20% Pl, and 5 to 10% Hbl and Bt (Fig. 3A). Small olivine crystals may be poikilitically enclosed by Opx or Cpx in these rocks. Both harzburgite and lherzolite contain small amounts of chrome spinel, most of which are generally enclosed within the olivine. Interstitial hornblende and biotite as well as plagioclase (totally less than 15 vol %) occur between granular olivine and pyroxene. The hornblende may also form the reaction rim of the pyroxene. Olivine gabbronorite with a thickness of 10 to 30 m overlies the lherzolite along the southwestern margins of the intrusion (Fig. 2). A 50- to ~300-m-long gabbro dike with a width of 1 to ~6 m occurs along the southwestern margin of the Heishan intrusion and shows sharp contacts with the lherzolite and gabbronorite (Fig. 2A).

The cumulus sequence from the base to the top of the Heishan intrusion (harzburgite→lherzolite→olivine gabbronorite) and the occurrence of the disseminated sulfides of the No. 4 orebody at the base of the intrusion suggest in situ fractional crystallization with gravitational accumulation (Fig. 2B). Xie (2012) proposed that the Heishan intrusion was originally sill-like and was tilted to the southeast on the south limb of an anticline formed during following collisional orogeny.

There are two lenticular Ni-Cu sulfide orebodies named the No. 1 and No. 4 ore bodies in the lower parts of the intrusion (Fig. 2B). The No. 1 orebody, located within the harzburgite, is comprised of sparsely disseminated sulfides (2–7 vol % sulfides; Fig. 4A). It is ~400 m long, ~100 to 400 m wide with thickness of up to 30 m, and dips southward to depths of 300 to 560 m; there are a few small mineralized bodies within the harzburgite as shown in Figure 2B. The No. 4 orebody is hosted in the lherzolite at the base of the intrusion and extends from the northwestern end to the middle part of the intrusion. The No. 4 orebody is larger and richer in sulfides than the No. 1 orebody and mineralized harzburgites. It is ~600 m long, ~400 to 600 m wide, and dips to depths of ~300 to 750 m southward. The thickness of the No. 4 orebody reaches 120 m in drill hole ZK803 at the northwest end and decreases toward southeast to reach 50 m in drill hole ZK1603. The orebody is dominantly comprised of disseminated sulfides (2–20 vol % sulfides; Figs. 2B, 4B). Thin net-textured sulfides and massive sulfide as thick as 2 m have been discovered at the base of the No. 4 orebody in drill hole ZK 803 in the northwestern part of the intrusion.

The sulfide aggregates are interstitial at the triple points between grains of olivine and pyroxene (Fig. 4C, E). With

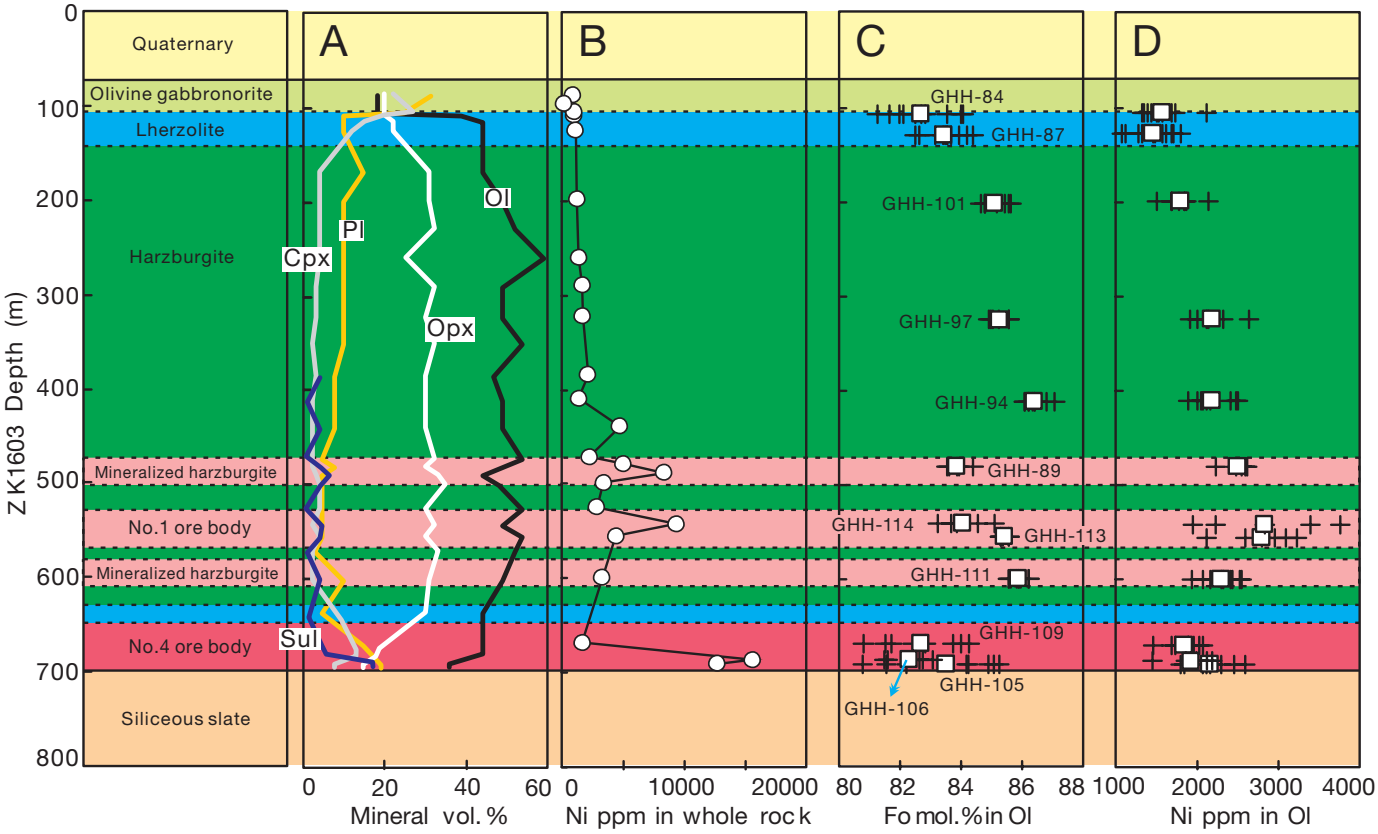

FIG. 3. Stratigraphic variations of (A) major rock-forming mineral volume percentage, (B) nickel content of the whole rock (data of the sulfide-poor rock is from Xie et al., 2012), (C) olivine forsterite content (Fo), (D) nickel content of the olivine from drill hole ZK1603 in the Heishan intrusion (Fig. 2). Black crosses represent analytical data and white boxes are for the average value of every sample. Abbreviations: Cpx = clinopyroxene, Ol = olivine, Opx = orthopyroxene, Pl = plagioclase, Sul = sulfide.

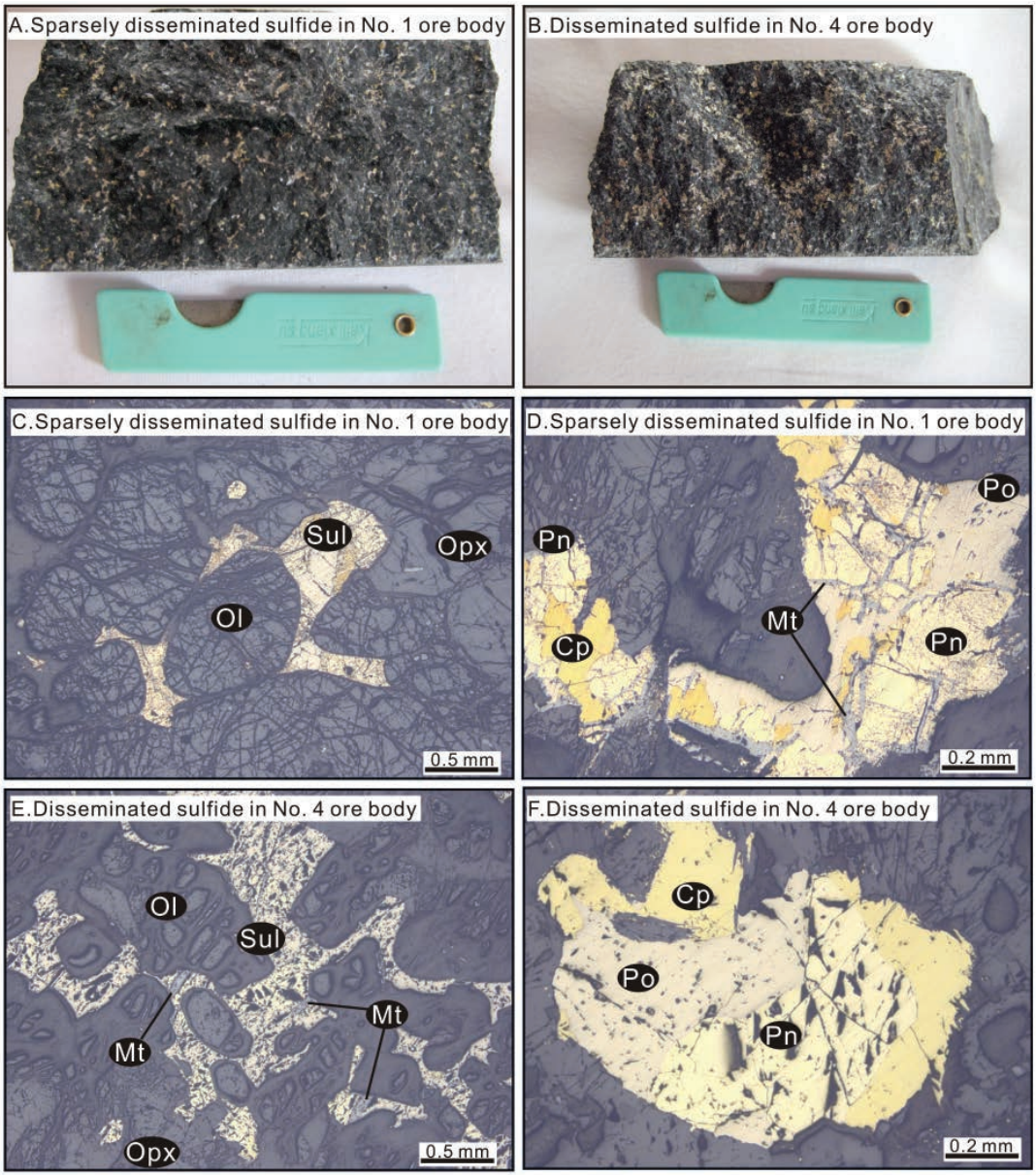

FIG. 4. Photos of drill core hand samples and reflected light photomicrographs from the Heishan intrusion. (A, B). Photos of drill core hand samples show that the samples are quite homogeneous. (C, E). Interstitial sulfide aggregates between the olivine crystals (×4 times). (D, F). Pentlandite crystals are subhedral or enclosed by anhedral pyrrhotite, anhedral chalcopyrite at margins of pyrrhotite or pentlandite, small veins of secondary magnetite cutting through base metal sulfides (×10 times). Abbreviations: Cp = chalcopyrite, Mt = magnetite, Ol = olivine, Opx = orthopyroxene, Pn = pentlandite, Po = pyrrhotite, Sul = sulfide.

increasing sulfide contents, the sulfides form poorly to moderately interconnected patches (up to 5 mm) of net-texture sulfide in the No. 4 orebody (Fig. 4E). The sparsely disseminated sulfides of the No. 1 orebody and mineralized harzburgites include 30 to 45 modal % pyrrhotite, 30 to 45 modal % pentlandite, and 20 to 30 modal % chalcopyrite, together with minor secondary magnetite occurring along fractures within the sulfides (Fig. 4D). The proportions of pyrrhotite, pentlandite, and chalcopyrite in the disseminated sulfides of the No. 4 orebody are 50 to 60 modal %, 20 to 30 modal %, and 15 to 25 modal %, respectively (Fig. 4F). Pentlandite crystals are commonlly subhedral or enclosed by anhedral or subhendral grains of pyrrhotite, or occur at boundaries or fractures of pyrrhotite grains. Anhedral chalcopyrite grains generally occur between the other sulfides or as very fine veinlets that crosscut the silicates. Secondary magnetite with minor content commonly occurs as small veins cutting through base metal sulfides (Fig. 4D, E). Cubanite or pyrite has not been found in the sulfides.

Sampling and Analytical Methods

Most of the samples were collected from drill cores ZK803 and ZK1603 that cross through the Heishan intrusion and a few from drill cores ZK1203 and ZK1403 and weakly weathered outcrop (Fig. 2). To avoid hand sample-scale heterogeneity,

each of our samples was combined by the fragments in ~2 m of the left cores and up to 600 to 800 g in weight. The entire sample was crushed with steel jaws to –10 mesh, and then ~200 g of this fraction were ground to –200 mesh powder using a tungsten carbide ring mill.

Platinum-group elements (PGE) were determined by isotope dilution (ID)-ICP-MS using an improved Carius tube technique (Qi et al., 2004, 2007). Five to 10 g and 3 to 5 g powder of sulfide-poor and sulfide-bearing samples, respectively, were used for analysis. The measured results of PGE for the reference standards TDB-1 and WGB-1 (Table 1) agree well with recommended values reported by Qi et al. (2004). Analytical precision and accuracy are generally better than 10% and the duplicate samples match each other very well (Table 2).

Nickel, Cu, Co, Cr, and Se, Te, As, Bi of the samples containing 3 to 20 vol % sulfides were measured using Varian ICP735-ES inductively coupled plasma emission spectrometer and Perkin Elmer Elan 9000 inductively coupled plasma mass spectrometer (ICP-MS), respectively, at the ALS Chemex (Guangzhou) Co. Ltd. Whole-rock S contents were measured using a gravimetric method and IR absorption in the Geological Analysis Central of the Metallogenic Geology Bureau of Southwest China with the detection limits ~0.01 wt %. The analytical precisions are ~8% for S, ~3% for Ni, Cu, Co, and Cr, and ~10% for As, Se, Te, and Bi.

Whole-rock sulfur isotope analyses of disseminated sulfides were performed on a Finnigan MAT 252 continuous flow isotope ratio mass spectrometry at the Institute of Geochemistry, Chinese Academy of Sciences, with an analytical uncertainty less than 0.2‰. Analyses of the GBW04414 S standard was –0.063‰ (n = 12). All sulfur isotope data are reported relative to V-CDT in standard δ notation.

Olivine compositions have been determined by wavelength-dispersive X-ray analysis using an EPMA-1600 electron microprobe at the Institute of Geochemistry, Chinese Academy of Sciences. The analytical conditions were beam current of 20 nA, acceleration voltage of 15 kV, and a beam size of 10 μm in diameter, and the counting time was 20 to 40 s for major elements and 40 to 60 s for minor elements. SPI (STRUCTURE PROBE Inc., Canada) mineral standards were used for calibration. Table 3 shows representative analyses (the complete dataset is available in the online data supplement).

Analytical Results

The forsterite percentages (Fo) of the olivine of the harzburgites (81–87%) are higher than Fo of the olivine of the lherzolites (77–85 %; Fig. 5A). Three evident reversals of Fo values of the olivine of the lherzolite and harzburgite can be identified (Fig. 3), although there is an overlap in olivine Ni contents of these rocks because of variable sulfide mineralization. The

TABLE 1. Blank and Analytical Results of Standard Materials WGB-1, TDB-1 for Platinum Group Elements

		WGB-1 (Gabbro)			TDB-1 (Diabase)		
	Blank	This study	Certified[1]	Certified[2]	This study	Certified[1]	Certified[2]
Ir	0.02	0.21	0.33	0.23	0.08	0.15	0.1
Ru	0.09	0.14	0.3	0.16	0.23	0.3	0.2
Rh	0.01	0.20	0.32	0.19	0.48	0.7	0.35
Pt	0.14	3.73	6.1	5.74	4.96	5.8	4.7
Pd	0.14	13.2	13.9	12	22.9	22.4	20.9

[1] Certified values are from Govindaraju (1994)
[2] Certified values are from Qi et al. (2004)

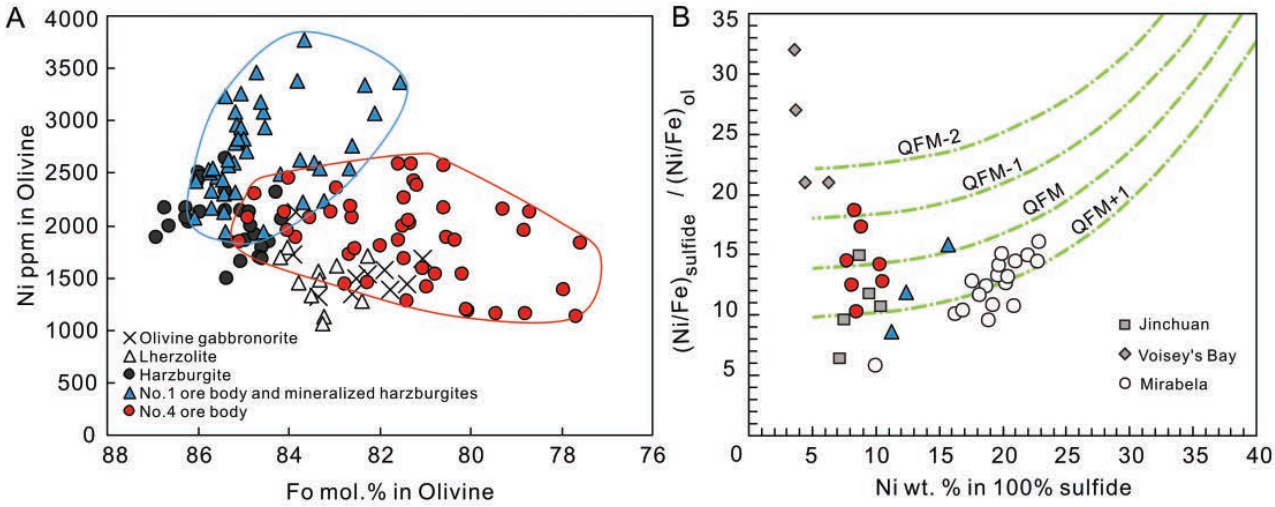

FIG. 5. (A). Plot of Ni vs. forsterite percentage (Fo) of olivine of the Heishan intrusion. (B). K_D ($(Ni/Fe)^{sulfide}/(Ni/Fe)^{olivine}$) as a function of wt % nickel in the sulfide liquid for olivine + sulfide-saturated intrusions (after Barnes et al., 2013). The data of Jinchuan and Voisey's Bay are from Brenan and Caciagli (2000); the data of Mirabela and the position of the K_D curves are from Barnes et al. (2013).

TABLE 2. Sulfur, Chalcophile, and Semimetal Element Concentrations and $\delta^{34}S$ of the Sulfides and Sulfide-Poor Rocks from the Heishan Intrusion

Sample	Rock type	Sulfide mineralization	Depth (m)	S (wt %)	MgO (wt %)	Cr (ppm)	Ni (ppm)	Cu (ppm)	Co (ppm)	Ir (ppb)	Ru (ppb)	Rh (ppb)	Pt (ppb)	Pd (ppb)	As (ppm)	Bi (ppm)	Se (ppm)	Te (ppm)	$\delta^{34}S$ (‰)
No.1 orebody and mineralized harzburgites																			
ZK1603																			
GHH-93	Harzburgite	Sp. disseminated	439	0.97	31.1	1,550	4,740	2,690	150	4.39	7.2	7.06	92.5	157		1.32	5.8	0.62	0.79
GHH-89	Harzburgite	Sp. disseminated	480	1.07	29.7	1,430	5,070	2,550	160						0.8	1.66	6.3	0.59	0.73
GHH-90	Harzburgite	Sp. disseminated	489	2.07	28.7	1,160	8,470	5,050	200	7.67	12.1	11.2	135	198		2.64	10.5	0.96	0.43
GHH-114	Harzburgite	Sp. disseminated	543	1.8	30.4	1,460	9,410	4,770	220	7.32	13.3	13.5	147	211	0.4	2.86	11.6	1.16	0.91
GHH-113	Harzburgite	Sp. disseminated	555	0.97	31.8	2,380	4,510	2,140	180	4.19	7.95	8.19	109	129	0.9	1.62	6.2	0.58	1.01
GHH-113[D]										3.10	7.71	6.37	114	130					
No.4 orebody																			
ZK1203																			
GHH-75	Lherzolite	Disseminated	763	2.40	31.8	1,310	7,370	4,560	230	3.18	8.51	5.67	60.2	74.2	0.3	2.34	9.4	0.66	1.9
GHH-75[D]										3.88	7.80	4.41	54.2	75.4					
ZK1603																			
GHH-106	Lherzolite	Disseminated	687	5.43	20.9	810	15,600	10,850	350	13.7	24.3	15.9	198	176	3.4	4.61	19.1	1.33	2.03
GHH-105	Lherzolite	Disseminated	690	4.16	20.7	860	12,800	7,340	260	11.9	20.5	11.5	129	104	7.6	2.86	13.6	0.96	2.14
ZK803																			
GHH-131	Lherzolite	Disseminated	464	1.56	25.9	1,120	4,570	2,360	170	3.64	8.68	4.01	36.2	37.9	1.2	1.07	4.8	0.33	3.7
GHH-129	Lherzolite	Disseminated	484	1.39	27.4	1,020													4.07
GHH-128	Lherzolite	Disseminated	490	2.24	26.3	970	6,270	3,500	190	3.84	9.55	5.28	52.3	72.4					3.77
GHH-126	Lherzolite	Disseminated	505	1.71	27.0	1,010	5,300	3,010	170	3.58	8.33	4.53	50.1	56.6					4.17
GHH-124	Lherzolite	Disseminated	513	3.73	24.6	850	10,150	8,490	270	5.16	8.69	6.06	150	147	4.3	5.2	14.5	1.38	3.05
GHH-125	Lherzolite	Disseminated	519	2.90	27.0	1,110	8,350	5,690	220	3.83	7.52	4.86	89.7	111	2.3	3.77	10.7	0.91	3.05
GHH-122	Lherzolite	Disseminated	525	2.64	20.9	810	6,350	4,350	190	3.88	9.53	4.98	48.5	67.5					3.75
GHH-120	Lherzolite	Disseminated	530	3.36	17.5	650	8,010	6,420	230	8.91	14.1	8.73	169	112					4.06
GHH-119	Lherzolite	Disseminated	535	4.65	17.5	720	11,000	7,280	310	14.4	25.5	12.9	72.9	110	9.3	3.59	12.7	0.89	4.44
GHH-119[D]										12.2	28.6	12.5	76.6	113					
GHH-118	Lherzolite	Disseminated	541	3.68	17.6	770	7,400	5,300	250	9.50	22.7	10.4	66.1	71	3.9	2.68	8.3	0.57	6.1
Sulfide-poor rock																			
ZK1403																			
GHH-30	Harzburgite		229		37.0	2,710	2,000	104	146	0.29	0.57	0.22	4.36	7.72					
ZK1203																			
GHH-50	Harzburgite		278		36.0	3,200	2,050	216	148	0.54	1.0	0.49	8.44	14.9					
ZK1603																			
GHH-82	Ol gabbronorite		85		23.1	1,690	1,000	446	108	0.07	0.14	0.09	1.11	1.76					
GHH-84	Ol gabbronorite		105		23.5	2,270	989	274	102	0.16	0.28	0.15	6.23	3.7					
GHH-85	Lherzolite		108		27.0	2,110	1,060	163	116	0.08	0.17	0.06	1.23	1.88					
GHH-87	Lherzolite		126		28.9	2,360	1,130	145	121	0.09	0.15	0.06	1.1	1.89					
GHH-101	Harzburgite		199		30.5	2,370	1,340	198	127	0.16	0.27	0.17	2.18	3.71					
GHH-99	Harzburgite		260		29.8	2,520	1,430	95	121	0.21	0.31	0.17	2.03	3.91					
GHH-98	Harzburgite		290		31.3	2,520	1,680	186	125	0.40	0.72	0.50	6.27	12.3					
GHH-94	Harzburgite		410		32.1	2,320	1,500	101	128	0.21	0.42	0.23	4.31	5.99					
ZK803																			
GHH-142	Ol gabbronorite		240		20.3	1,350	844	92	93	0.15	0.23	0.06	1.36	1.19					
GHH-141	Ol gabbronorite		270		20.7	1,390	901	124	93	0.14	0.27	0.11	1.41	1.82					
GHH-141[D]										0.13	0.34	0.08	1.42	1.69					
GHH-140	Lherzolite		298		24.0	1,660	1,230	183	112	0.34	0.49	0.21	3.16	3.66					
GHH-139	Lherzolite		313		25.6	1,770	1,480	255	121	0.45	0.71	0.24	3.15	5.02					
GHH-138	Lherzolite		319		26.8	1,800	1,330	191	117	0.31	0.62	0.25	3.42	4.07					
GHH-133	Lherzolite		416		27.1	1,810	1,590	305	121	0.56	1.19	0.48	7.44	7.57					

Notes: Ol = olivine, Sp = sparsely; samples labeled with "[D]" are duplicates reanalyzed for PGE

Table 3. Representative Olivine Contents from the Heishan Sulfide-Poor and Sulfide-Bearing Rocks

Spot	Depth m	Situation	SiO_2 (wt %)	TiO_2 (wt %)	Al_2O_3 (wt %)	Cr_2O_3 (wt %)	FeO (wt %)	MnO (wt %)	MgO (wt %)	NiO (wt %)	CaO (wt %)	Total (wt %)	Fo (mol %)	Ni (ppm)
Olivine gabbronorite														
GHH-84														
OL-6	105	Sil-contact	39.3	0.01	0.02	0.02	17.0	0.24	41.4	0.21	0.11	98.3	81.1	1,683
OL-9	105	Sil-contact	39.2	0.03	0.02	0.01	14.8	0.20	44.0	0.22	0.13	98.6	83.9	1,723
Lherzolite														
GHH-87														
OL-10	126	Sil-contact	40.9	0.01	0	0.03	14.4	0.24	43.9	0.22	0.19	99.9	84.2	1,691
OL-11	126	Sil-contact	39.9	0.03	0	0.07	16.2	0.21	42.7	0.22	0.21	99.6	82.3	1,707
Harzburgite														
GHH-101														
OL-5	199	Sil-contact	41.3	0.03	0	0.04	13.5	0.21	45.0	0.19	0.14	100.5	85.4	1,495
OL-6	199	Sil-contact	40.3	0.02	0.02	0.01	14.1	0.20	43.5	0.23	0.13	98.5	84.4	1,841
GHH-94														
OL-1	410	Sil-contact	40.6	0.01	0	0.01	12.1	0.19	45.8	0.24	0.13	99.1	86.9	1,888
OL-6	410	Sil-contact	40.2	0.03	0	0	13.1	0.18	45.6	0.27	0.09	99.5	86.0	2,124
Harzburgite, sparsely disseminated														
GHH-89														
OL-4	480	Sil-contact	40.1	0.01	0.01	0.02	14.6	0.27	44.5	0.32	0.14	100.0	84.2	2,486
OL-10	480	S-contact	40.0	0.05	0	0.01	17.0	0.21	42.6	0.43	0.07	100.3	81.6	3,367
GHH-111														
OL-1	600	Sil-contact	40.5	0.03	0	0.04	12.9	0.16	45.3	0.31	0.09	99.3	86.1	2,423
OL-12	600	Sil-contact	40.2	0.03	0	0	14.2	0.13	43.9	0.37	0.10	98.9	84.5	2,934
Lherzolite, disseminated														
GHH-106														
OL-2	687	S-contact	40.3	0.13	0.00	0.02	16.6	0.22	41.6	0.25	0.12	99.4	81.5	1,988
OL-5	687	S-contact	40.5	0.03	0.01	0.03	15.4	0.21	43.0	0.27	0.16	99.7	83.1	2,130
GHH-105														
OL-2	690	Sil-contact	41.0	0.02	0	0.03	13.9	0.20	44.9	0.24	0.16	100.4	85.1	1,849
OL-4	690	S-contact	38.7	0	0.01	0	17.7	0.22	41.6	0.28	0.14	98.6	80.6	2,171
GHH-131														
OL-2	464	S-contact	39.6	0.04	0.05	0.03	17.6	0.25	40.6	0.20	0.14	98.5	80.2	1,532
OL-4	464	S-contact	40.0	0.03	0.03	0.02	15.9	0.20	42.8	0.23	0.17	99.4	82.6	1,784
GHH-124														
OL-4	513	S-contact	39.8	0.01	0.00	0.02	18.2	0.26	39.7	0.27	0.14	98.5	79.3	2,153
OL-5	513	S-contact	39.5	0.06	0.04	0.09	17.9	0.21	43.6	0.20	0.18	101.9	81.1	1,595
GHH-119														
OL-1	535	S-contact	39.5	0.04	0.02	0.02	18.5	0.26	39.0	0.15	0.19	97.7	78.8	1,163
OL-3	535	S-contact	40.1	0.00	0.02	0.03	19.9	0.25	39.2	0.23	0.19	99.9	77.6	1,831

S-contact = olivines are contact with sulfides, Sil-contact = olivines are contact with silicate minerals

olivines in the No. 1 orebody and mineralized harzburgites have higher Fo (81.6–86.1%) and Ni (1,940–3,770 ppm) than the olivines in the disseminated sulfides of the No. 4 orebody (Fo = 77.6–85.1% and Ni = 1,130–2,590 ppm; Figs. 3, 5A).

The whole-rock contents of Ni, Cu, Co, and PGE of the Heishan rocks and sulfides are listed in Table 2. The olivine gabbronorite, lherzolite, and harzburgite contain 840 to 2,050 ppm Ni, 90 to 450 ppm Cu, and 90 to 150 ppm Co, respectively. These rocks generally have <1 ppb Ir, Ru, and Rh, <9 ppb Pt, and <15 ppb Pd, respectively (Table 2). Particularly, the sulfide-poor rocks display positive correlations between Ni and MgO and Cr, whereas Ni is negatively correlated to MgO and Cr in the sulfides (Fig. 6). Positive correlation between Ni and MgO and Cr suggests that Ni is mainly contained by olivine in these rocks (Fig. 6C, D). On primitive mantle-normalized diagrams, these rocks have the similar pattern with depletion in IPGE (Ir, Ru), enrichment in PPGE (Rh, Pt, Pd), and Ni and Cu (Fig. 7A). The metal and semimetal elements of the sulfides in the Nos. 1 and 4 orebodies and mineralized harzburgites are much richer than the sulfide-poor rocks, indicating that these elements are mainly contained by sulfides (Table 2). These elements show good positive correlations with S in the sulfides (Fig. 8). The positive intercepts of Co for both Nos. 1 and 4 orebodies on the Co versus S plot is due to Co being compatible to olivine and pyroxene (Fig. 8C), whereas the negative intercept of As in the diagram of As versus S probably indicates a loss of As during analysis (Fig. 8G).

Before the 100% sulfide recalculation using the methods proposed by Barnes et al. (2011), silicate nickel in the disseminated sulfides has been calculated based on the correlation between the contents of Ni and MgO of the sulfide-poor samples containing <1 vol % sulfide and <200 ppm Cu (Fig. 6C). The sparsely disseminated sulfides of the No. 1 orebody and

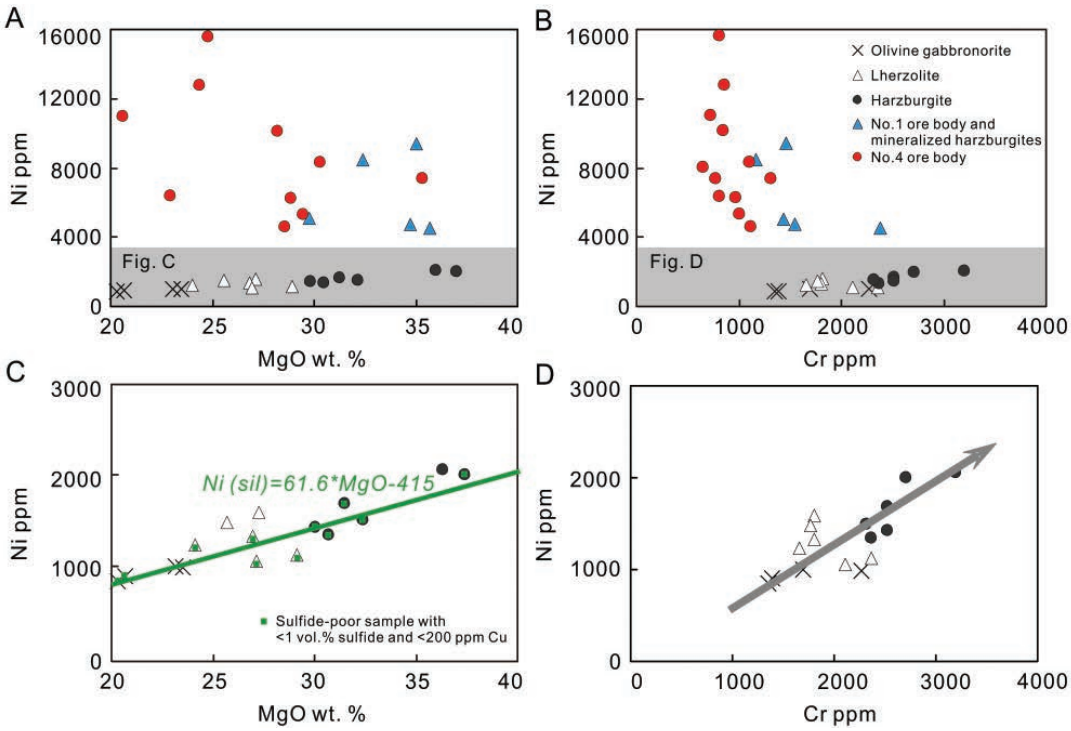

FIG. 6. Plots of MgO vs. Ni (A, C) and Cr vs. Ni (B, D) for the mineralized and sulfide-poor rocks from the Heishan intrusion.

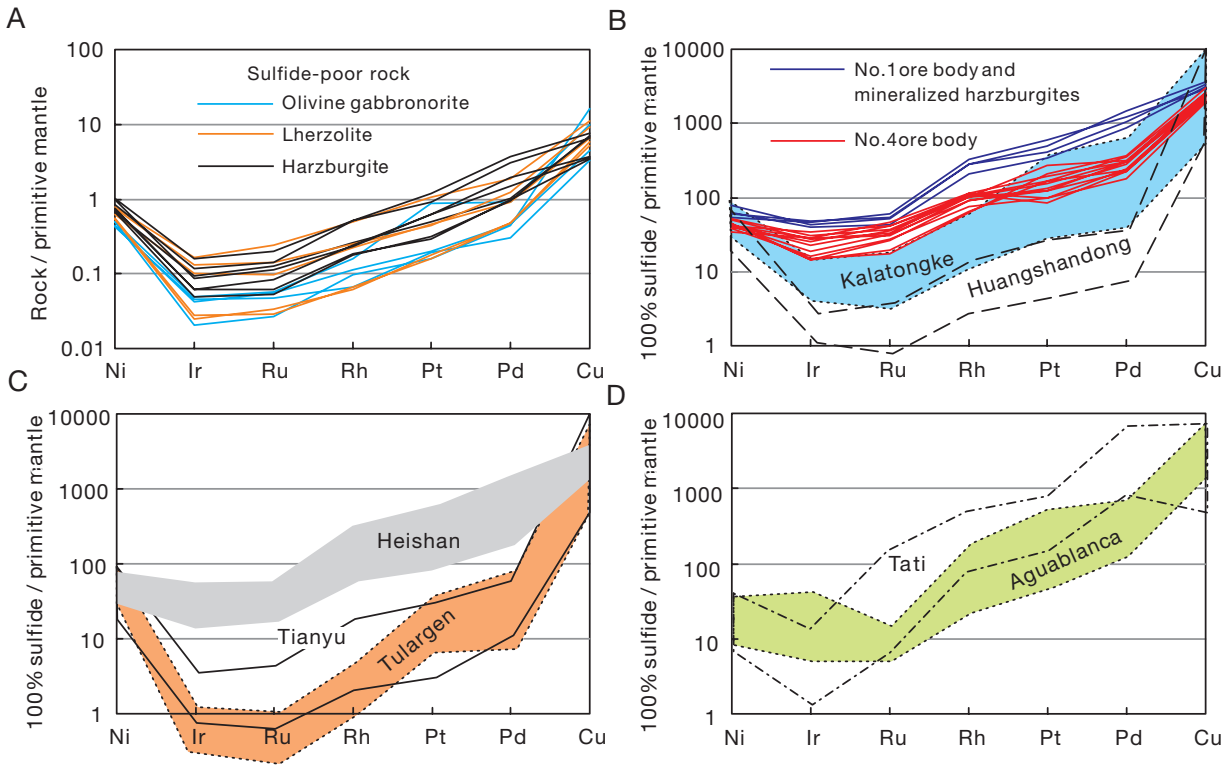

FIG. 7. (A). Primitive-mantle normalized Ni, PGE, and Cu patterns of the Heishan sulfide-poor rock samples. (B, C, D) Primitive-mantle normalized Ni, PGE and Cu patterns of the sulfides of the Heishan deposit on a 100% sulfide basis. Primitive mantle values of Ni, PGE and Cu used in the normalization are from Barnes and Maier (1999). The field for disseminated sulfides of Kalatongke, Huangshandong, Tulargen and Tianyu are from Song and Li (2009), Li et al. (2012), Sun et al. (2013), Deng et al. (2014), Jiao et al. (2012) and Tang et al. (2011), respectively. The values of the disseminated sulfides of the Aguablanca and Tati deposits are from Piña et al. (2008) and Maier et al. (2008), respectively.

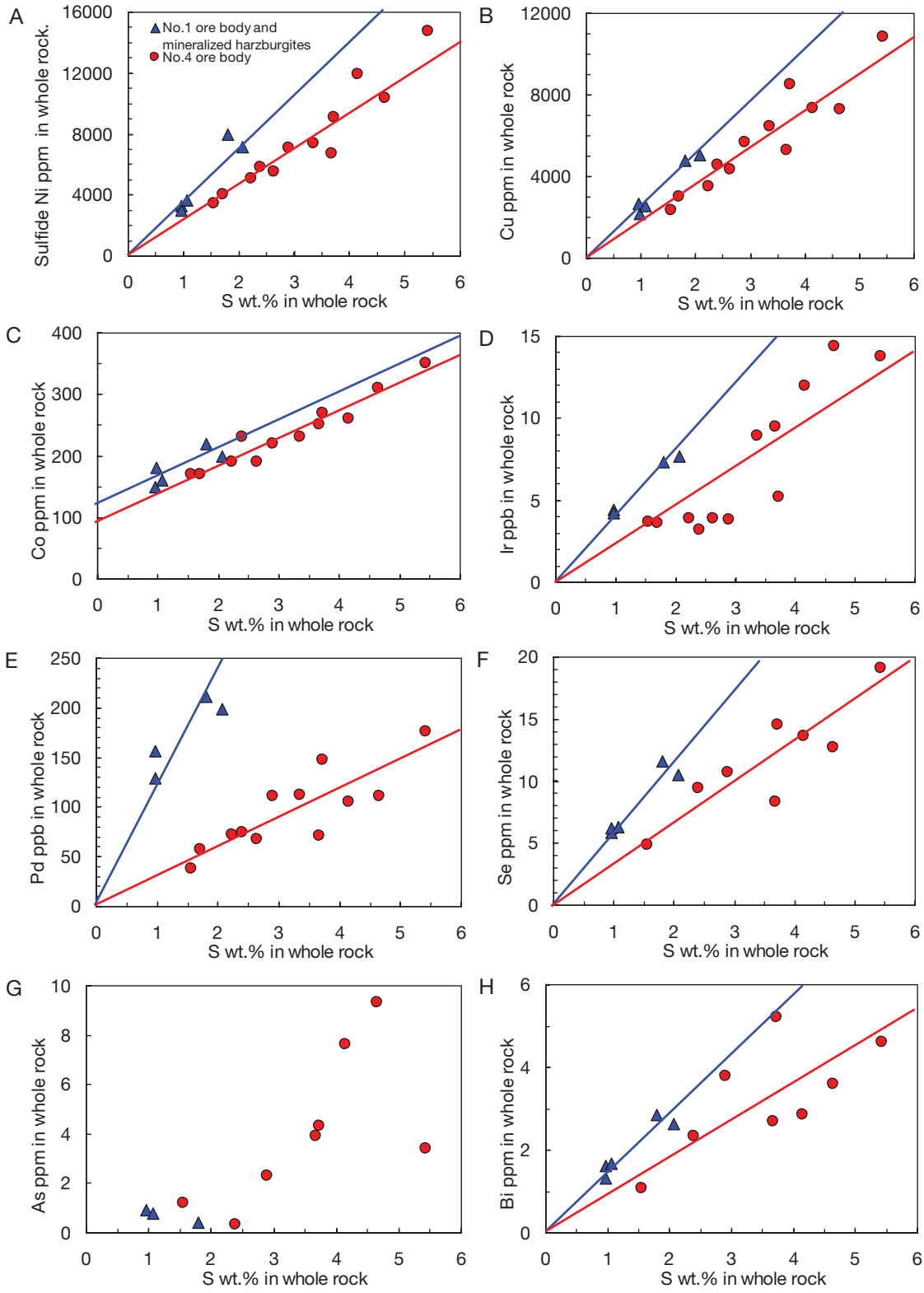

FIG. 8. Sulfur vs. sulfide nickel after subtracting the silicate background, other chalcophile and semimetal elements in whole rock for the sulfides of the Heishan deposit. Linear regression lines are shown for the No. 1 orebody and mineralized harzburgites (blue) and the No. 4 orebody (red).

mineralized harzburgites contain as high as 11.2 to 15.6 wt % Ni, 8.1 to 10 wt % Cu, 130 to 160 ppb Ir, 2,350 to 4,110 ppb Pt, and 3,460 to 5,840 ppb Pd, with 16,000 to 26,000 Cu/Pd ratios on a 100% sulfide base (Fig. 9). Although the disseminated sulfides of the No. 4 orebody contain more sulfides, they contain relatively lower chalcophile elements and higher Cu/Pd ratios (48,000–75,000) on a 100% sulfide basis, such as 6.9 to 10.5 wt % Ni, 5.4 to 8.4 wt % Cu, 50 to 120 ppb Ir, 580 to 1,860 ppb Pt, and 720 to 1,450 ppb Pd (Fig. 9). The No. 1 sparsely disseminated sulfides and mineralized harzburgites also are higher in Se, Bi, and Te than the No. 4 disseminated sulfides.

In a primitive mantle-normalized diagram, the No. 1 sparsely disseminated sulfides and mineralized harzburgites are similar to the No. 4 disseminated sulfides; they are enriched in Cu and PPGE and depleted in Ni and IPGE (Fig. 7B). The Heishan disseminated sulfides are less depleted in PGE relative to Ni and Cu than the disseminated sulfides of the Kalatongke, Tulargen, Tianyu, Huangshandong, and Tulargen deposits (Fig. 7B, C; Song and Li, 2009; Tang et al., 2011; Gao et al., 2012; Jiao et al., 2012; Li et al., 2012; Sun et al., 2013; Deng et al., 2014). The PGE contents of the Heishan sulfides are similar to those of the disseminated sulfides of the Tati deposit (Maier et al., 2008) and slightly higher in abundance than those of the Aguablanca deposit (Piña et al., 2008; Fig. 7D).

The sparsely disseminated sulfides of the No. 1 orebody and mineralized harzburgites have lower $\delta^{34}S$ values (0.43–1.01‰) and higher Se/S ratios (590–640 × 10^{-6}) than the sulfides of the No. 4 orebody, which have $\delta^{34}S$ of 1.9 to 6.1‰ and Se/S of 230 to 390 × 10^{-6} (Fig. 10A, B; Table 2). In conclusion, the sulfides of the No. 1 orebody and mineralized harzburgites are characterized by higher contents of PGE and semimetal elements, lower Cu/Pd ratios, lower $\delta^{34}S$ values, and higher Se/S ratios than those of the No. 4 orebody.

Discussion

Economically extractable metals in magmatic Ni-Cu-(PGE) deposits have been discovered in a few orogenic belts around the world; these include the Tati and Selebi-Phikwe deposits in Botswanna, and the Aguablanca deposit in southwestern Spain, indicating exploration opportunity in convergent tectonic settings (Casquet et al., 2001; Piña et al., 2006; Maier et al., 2008). The discovery of the Heishan Ni-Cu-(PGE) deposit hosted in a Late Devonian intrusion (357 ± 4 Ma) indicates that the magmatic sulfide mineralization along the southern margin of the Central Asian orogenic belt can be formed in subduction environments, although most of the magmatic Ni-Cu-(PGE) deposits hosted in Permian mafic-ultramafic intrusions were concerned to be associated with postsubduction magmatism (Song and Li, 2009; Song

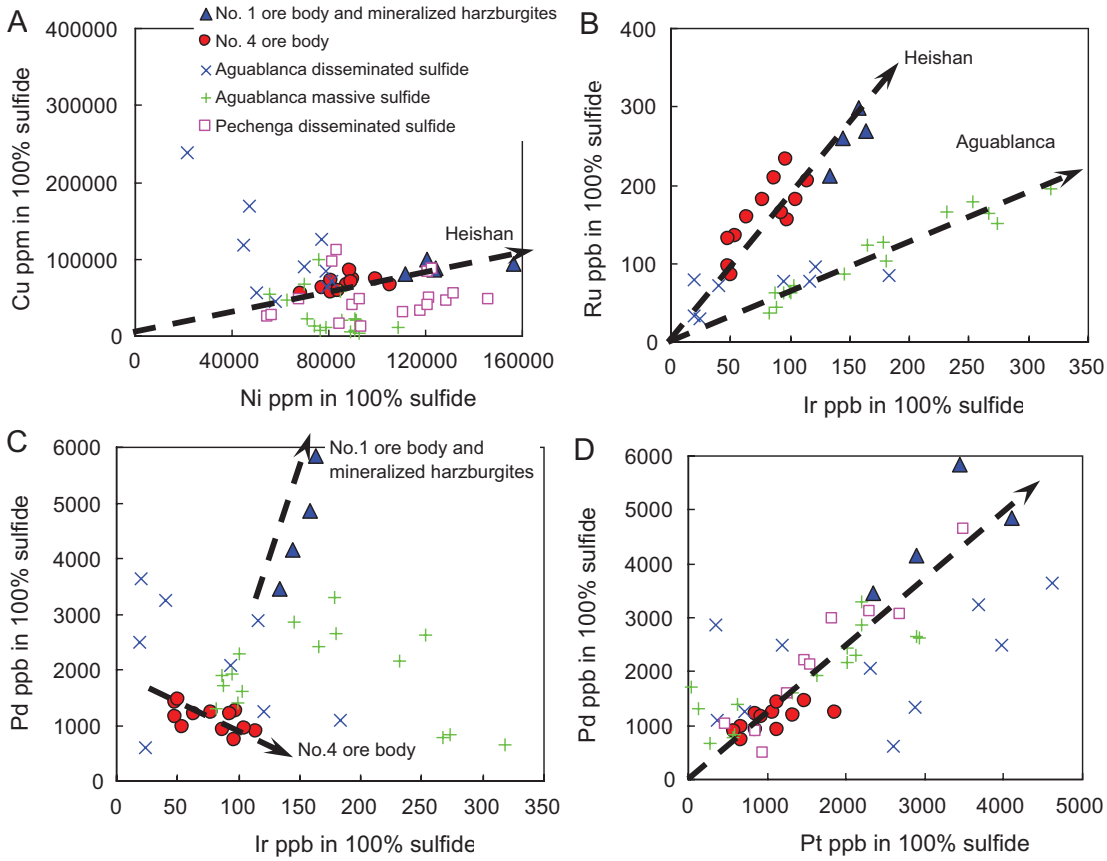

FIG. 9. Plots of platinum group elements of the Heishan sulfides (No. 1 orebody and mineralized harzburgites and No. 4 orebody) on a 100% sulfide basis. The values of the sulfides of the Pechenga and Aguablanca deposits are from Hanski et al. (2011) and Piña et al. (2008), respectively. We use the formula by Barnes and Lightfoot (2005) to recalculate the element contents to 100% sulfide basis.

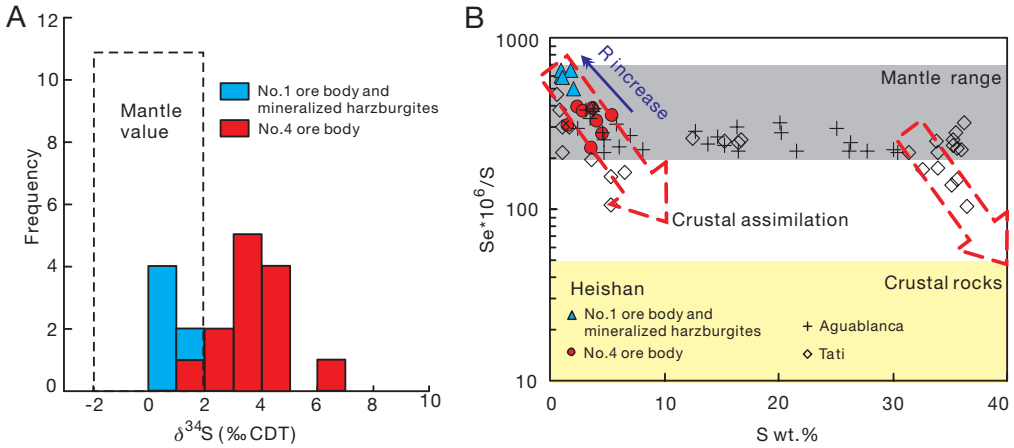

FIG. 10. (A). Sulfur isotope data from the sulfides of the Heishan deposit. (B). Plot of Se*10⁶/S vs. S for the Heishan disseminated sulfides. The values of the sulfides of the Aguablanca and Tati deposits are from Piña et al. (2008) and Maier et al. (2008), respectively.

et al., 2011, 2013; Li et al., 2012; Xie et al., 2012; Sun et al., 2013; Xia et al., 2013).

Devonian-Carboniferous calc-alkaline basaltic andesite, dacite, and rhyolite as well as 378 to 328 Ma gabbro-diorite intrusions are widespread in the Beishan fold belt at the northern Tarim (BGMRG, 1989; Chen et al., 1999; Hu et al., 2000; Charvet et al., 2007; Zhang and Guo, 2008; Liu et al., 2011). The Devonian calc-alkaline andesites located at ~50 km to the east of the Heishan intrusion show extensive Nb and Ta depletion and enrichment of large ion lithophile elements and plot in the field of island-arc basalts in the Th-Hf-Nb diagram, indicating the subduction-related magmatism (Xie et al., 2012). This again demonstrates that the Beishan fold belt was an active continental margin in the Devonian-Carboniferous and the calc-alkaline volcanics was associated with S-dipping subduction of the South Tianshan Ocean in the Late Paleozoic (Chen et al., 1999; Charvet et al., 2007; Zhang and Guo, 2008; Liu et al., 2011). Our recent SHRIMP U-Pb dating (357 ± 4 Ma) and ID-TIMS U-Pb dating (356.4 ± 0.6 Ma) of zircons from gabbros confirmed that the Heishan intrusion was formed concurrently with the Devonian calc-alkaline volcanics in the Beishan fold belt (Xie et al., 2012). The Heishan intrusive rocks also show enrichments of large ion lithophile elements, strong negative Nb (Ta) anomalies, and positive K and Pb anomalies in an N-MORB normalized trace element diagram (Xie et al., 2012). Additionally, The Heishan intrusive rocks plot together with volcanics of active continental margins, such as the volcanics along the Pacific margins of the Americas, in the diagrams of $\varepsilon Nd_{(t)}$ versus $(^{87}Sr/^{86}Sr)_t$ and diagrams of lead isotopes (Xie et al., 2012). Clinopyroxenes of the Heishan sulfide-free rocks fall in the overlay region of N-MORB and back-arc basin basalt, indicating that the magma was derived from partial melting of the asthenosphere and mantle wedge triggered by upwelling of asthenosphere due to break-off of subduction slab (Xie et al., 2012).

The chalcophile element abundance of magmatic sulfides is controlled by several processes; the important factors are (1) the concentrations of these elements in the parental silicate magma, (2) partitioning of these elements between sulfide liquid and silicate magma, (3) fractional crystallization of the sulfide liquid, and (4) late hydrothermal alteration (e.g., Campbell and Naldrett, 1979; Naldrett and Barnes, 1986; Keays, 1995; Ebel and Naldrett, 1996; Barnes et al., 1997; Naldrett, 1999; Crocket, 2002; Barnes and Lightfoot, 2005). In the following parts, we focus on the factors controlling the formation of the Heishan sulfide mineralization using the data described above.

The data presented so far indicate that the correlation of Pt versus Pd in sulfide-poor mafic-ultramafic rocks is dominantly controlled by original crystallization and accumulation of olivine and in disseminated sulfides by the abundance of sulfide regardless of degree and style of alteration (Barnes et al., 2009; Barnes and Liu, 2012). Although the occurrence of secondary magnetite occurring along fractures within the sulfides indicates that the Heishan sulfides have been modified by hydrothermal alteration (Fig. 4D, E), the positive correlation of Pt and Pd of the Heishan disseminated sulfides (Fig. 9D) indicates that they are controlled by the abundance of sulfide. In addition, the ratios of Ir/(Ir + Ru) and Pt/(Pt + Pd) (0.26–0.39 and 0.37–0.6, respectively) are typical of magmatic sulfide (Ir/(Ir + Ru) = 0.3–0.7, Pt/(Pt + Pd) = 0.3–0.7; Naldrett et al., 1982), indicating that hydrothermal alteration has a limited effect on the PGE compositions of the Heishan disseminated sulfides.

Different sulfide liquids of the No. 1 and No. 4 orebodies

Although the No. 4 orebody has higher sulfide contents than the No. 1 orebody and mineralized harzburgites (Fig. 8), the PGE content in 100% sulfides of the No.4 orebody (50–120 ppb Ir, 580–1,860 ppb Pt, and 720–1,450 ppb Pd) are lower than those of the No.1 orebody (130–160 ppb Ir, 2,350–4,110 ppb Pt, and 3,460–5,840 ppb Pd; Table 2, Fig. 9). The sulfides from these two orebodies and mineralized harzburgites have different compositions and plot in the trends having different slopes to the origin in the diagrams of Ni, Cu, PGE, Se, and Bi against S (Fig. 8). On a 100% sulfide basis, the sulfides from the No. 1 orebody and mineralized harzburgites show positive correlations between PPGE and IPGE, indicating the sulfide liquids have not experienced evident fractionation (Fig. 9). In contrast, the negative

correlations between PPGE and IPGE of the No. 4 orebody indicate fractional crystallization of monosulfide solid solution (MSS; Fig. 9C).

It is well known that both Fo and Ni contents of olivine decrease during fractional crystallization, whereas equilibration of olivine with coexisting sulfide liquid will result in elevation of Ni contents of the olivine according to the exchange partition coefficient $K_D = (Ni/Fe)^{sulfide}/(Ni/Fe)^{olivine}$ (e.g., Barnes and Naldrett, 1985; Li and Naldrett, 1999; Brenan and Caciagli, 2000). The correlations between Ni and Fo of olivines in the Heishan sulfides indicate Fe-Ni exchange between the olivine and the sulfide (Fig. 5A). The relatively higher Fo and Ni contents of the olivine crystals in the No. 1 orebody and mineralized harzburgites (Fo = 81.6–86.1%; Ni = 1,930–3,770 ppm) are higher than those of the olivines in the No. 4 orebody (Fo = 77.6–85.1% and Ni = 1,130–2,590 ppm) indicate that the former reacted with a sulfide liquid more enriched in Ni through reaction with more primitive magmas (Fig. 5A).

Sulfide segregation resulted from assimilation of crustal sulfur

Previous studies have confirmed that assimilation of crustal sulfur is critical for sulfide immiscibility of mantle-derived magma and the formation of magmatic Ni-Cu-(PGE) deposits (e.g., Naldrett, 1999, 2010; Ripley and Li, 2003; Barnes and Lightfoot, 2005 and references therein), although the sulfides of some magmatic sulfide deposits (such as the Nebo-Babel deposit) have mantle-like sulfur isotope values (Seat et al., 2009, 2011). Despite the $\delta^{34}S$ data of the No. 1 orebody and mineralized harzburgites (0.43–1.01‰) fall within the accepted mantle range of 0 ± 2‰ (Fig. 10A), higher $\delta^{34}S$ values (1.9–6.1‰) of the disseminated sulfides of the No. 4 orebody indicate that crustal sulfur has played a more important role in the formation of the sulfides (Fig. 10A).

Typically, the Se/S ratios of mantle-derived rocks are ~230 to 350 × 10^{-6}, whereas crustal rocks tend to have much lower values of Se/S (<50 × 10^{-6}; Eckstrand et al., 1989; McDonough and Sun, 1995; Peltonen, 1995; Lorand et al., 2003). Sulfides which contain a large contribution of crustal sulfur tend to have low Se/S ratios at relatively high sulfide contents and low Pt + Pd contents in 100% sulfides due to more extensive sulfide segregation (e.g., Peltonen, 1995; Thériault and Barnes, 1998; Lorand et al., 2003; Godel and Barnes, 2008; Queffurus and Barnes, in press) because Se can substitute for S in sulfide as a chalcophile element (Paktunc et al., 1990; Czamanske et al., 1992; McDonough and Sun, 1995; Dare et al., 2010b). In the case of the Heishan sulfides, crustal assimilation is indicated by the negative correlations between S and Se/S, although the Se/S ratios (230–640 × 10^{-6}) are comparable with those of the mantle (Fig. 10B). Sulfides from the Aguablanca deposit in southwestern Spain and the Tati deposit in Botswanna also have high Se/S ratios (Fig. 10B; Maier et al., 2008; Piña et al., 2008). The negative correlation between Se/S and $\delta^{34}S$ and the positive correlation of Se/S and Cu/Pd in the disseminated sulfides of the No. 4 orebody indicate the synergistic effect of crustal sulfur input and variable degrees of the sulfide segregation and fractionation (Fig. 11A, B).

Fractional crystallization under S-unsaturated conditions, ratios of PPGE and incompatible elements in magma, such as Pt/Zr, remain constant because PPGE are also incompatible to silicates, whereas the PPGE/Ti ratio increases before crystallization of Fe-Ti oxides because Ti is moderately incompatible for pyroxene (Puchtel and Humayuan, 2001; Righter et al., 2004; Song et al., 2008, 2009a; Fiorentini et al., 2010). Once S saturation is achieved in the magma, the ratios of Pd/Ti and Pt/Zr will be dramatically reduced because of the removal of dense sulfide (e.g., Keays and Lightfoot, 2007; Song et al., 2009a; Fiorentini et al., 2010). Correlations between Pd/Ti and Pt/Zr in the barren rocks of the Heiahan intrusion indicate that their parental magma experienced sulfide segregation at different stages in the evolution of the magma (Fig. 12A).

Variable chalcophile element composition of parental magmas

The Ni/Cu and Pd/Ir ratios of the Heishan sulfides ranging from 1.06 to 1.65 and from 7.5 to 35.6, respectively, which

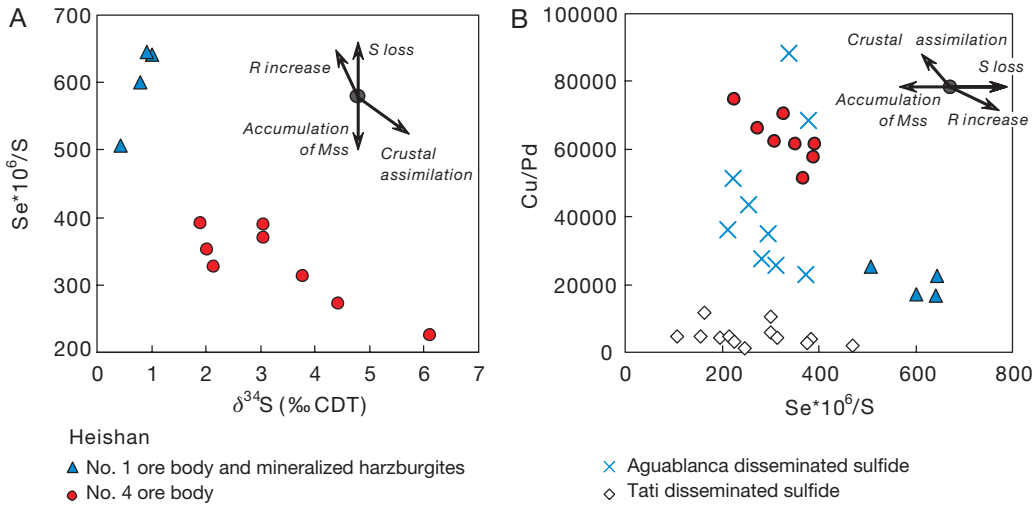

FIG. 11. Plots of (A) $\delta^{34}S$ vs. Se*10^6/S and (B) Se*10^6/S vs. Cu/Pd for the Heishan sulfides (No. 1 orebody and mineralized harzburgites and No. 4 orebody). The values of the Aguablanca and Tati disseminated sulfides are from Piña et al. (2008) and Maier et al. (2008), respectively.

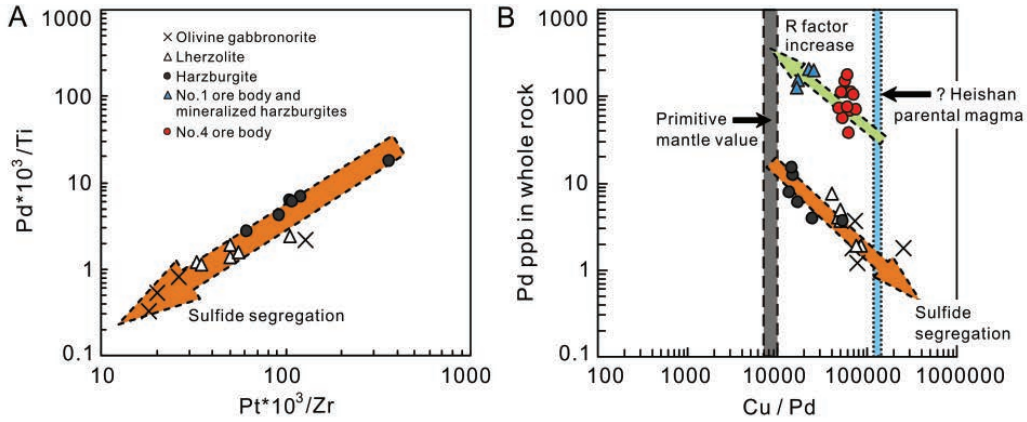

FIG. 12. (A). Ratio plot of Pd*10³/Ti vs. Pt*10³/Zr for the Heishan sulfide-poor rocks. (B). Plot of Pd vs. Cu/Pd for the sulfide-poor rocks and the sulfides of the Heishan intrusion.

indicates that the sulfides segregated from a high Mg basaltic magma (Fig. 13; e.g., Barnes et al., 1988; Naldrett, 2004; Barnes and Lightfoot, 2005). The sulfides of the No. 1 and No. 4 orebodies have Cu/Pd ratios of 16,000 to 26,000 and 48,000 to 75,000, respectively. Correspondingly, the calculated Cu/Pd ratios of their parental magmas according to the equation proposed by Campbell and Barnes (1984) should be as high as 18,000 to 93,000 and 48,000 to 214,000, respectively, which is much higher than Cu/Pd ratio of the primitive mantle (7,000–10,000, Barnes et al., 1993). Our model calculation uses the equation proposed by Campbell and Naldrett (1979). The model indicates that the disseminated sulfides of the No. 1 and No. 4 orebodies and mineralized harzburgites are plausibly segregated from the same parent magma weakly depleted in PGE, which contained 120 ppm Cu, 0.04 ppb Ir, and 1 ppb Pd under R factors of 700 to 1,600 and 4,000 to 8,000, respectively (Fig. 14A, B; where the R factor is mass ratio of silicate magma to sulfide melt). This is consistent with evidence that the olivines in the No. 1 orebody and mineralized harsburgite have higher Ni contents than those in the No. 4 orebody (Fig. 5A). In the calculations, the partition coefficients of Cu, Ir, and Pd ($D_i^{sul/sil}$) are assumed to be 1,000, 30,000 and 40,000, respectively (Peach et al., 1990; Stone et al., 1990; Fleet et al., 1993; Bezmen et al., 1994; Crocket et al., 1997; Ripley et al., 2002; Sattari et al., 2002).

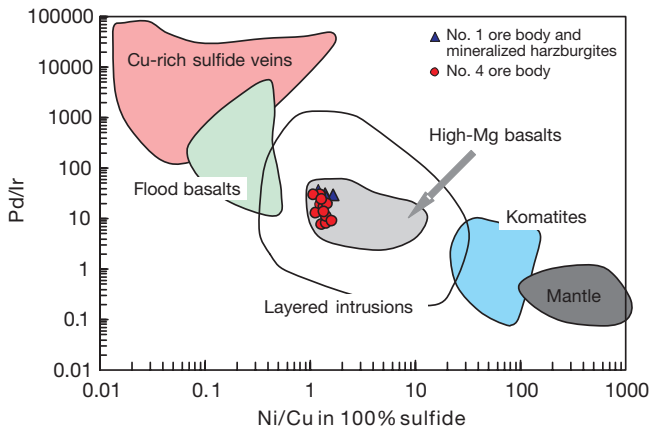

FIG. 13. Ratio plots of Ni/Cu vs. Pd/Ir (simplified diagram after Barnes et al., 1988) for the sulfides of the Heishan deposit.

Based on the characteristics of whole-rock trace elements, Sr-Nd-Pd isotopes and composition of clinopyroxene, Xie et al. (2012) proposed that the Heishan magma was generated by partial melting of the asthenosphere and mantle wedge due to slab break-off at an active continental margin. Copper may be enriched in the mantle wedge because of uprising of Cu-enriched fluids and/or melts from subducted slab (McDonough and Sun, 1995; Heinrich et al., 1999; Seedorff et al., 2005; Sun et al., 2011). Arc lavas other than boninites produced by melting of the mantle wedge are commonly high in Cu and low in PGE contents, probably because of sulfide retention in the mantle due to the low degree of partial melting or originally PGE depletion in the mantle wedge (Brandon et al., 1996; Rehkämper et al., 1997; McInnes et al., 1999). For instance, the Grenada and Izu-Bonin arc picrites contain much lower PGE (<0.2 ppb Ir, 1–4 ppb Pd) than komatiites and plume-related picrites (Woodland et al., 2002). The magmas derived from the mantle wedge along arcs or active continental margins are commonly high in oxygen fugacity relative to the intraplate magmas and middle oceanic ridge basaltic magmas (e.g., Botcharnikov et al., 2010; Evans et al., 2012). The mantle-like $\delta^{34}S$ values of the sulfides (0.43–1.01‰) from the No. 1 orebody and mineralized harzburgites and high Fo olivine contained in the harzbiurgites indicate that the sulfides were segregated from weakly crustal contaminated and more primary magma (Figs. 5A, 10). The K_D values of the No. 1 orebody and mineralized harzburgites and No. 4 orebody indicatethe the f_{O_2} of the Heishan parental magma is within a log unit of QFM (Fig. 5B), which is well within the limit for S to dissolve in the magma as sulfide. Such oxygen fugacity range is similar to that of the Jinchuan sulfides and higher than that of the Voisey's Bay sulfides (Brenan and Caciagli, 2000). This indicates that the Heishan sulfides were segregated from the evolved magma with normal oxygen fugacity.

Therefore, the PGE depletion of the Heishan parental magma was probably inherited from the primary magma derived from the asthenosphere and mantle wedge or resulted from prior weak sulfide segregation. The low Cu/Pd ratios of

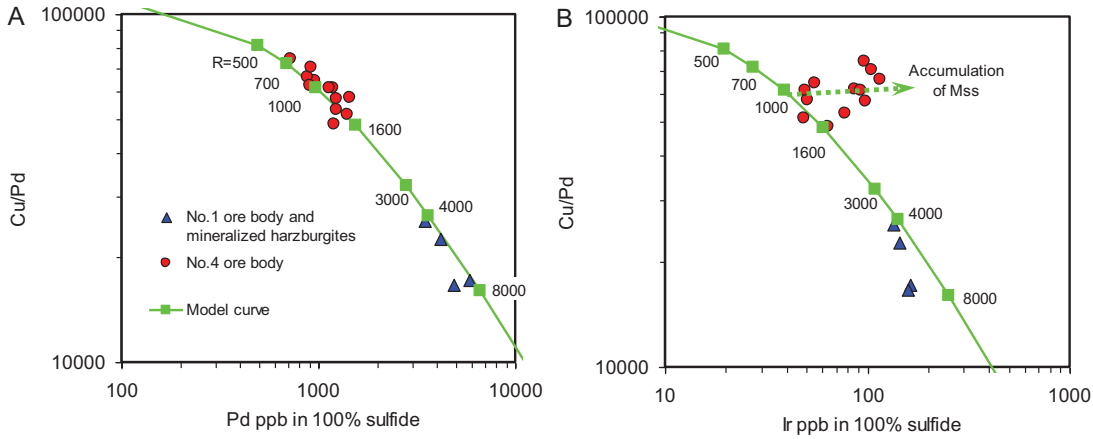

FIG. 14. Plots of the Heishan sulfides in (A) Cu/Pd vs. Pd and (B) Cu/Pd vs. Ir in sulfide melt. Model curve displays the compositional variation of the sulfide melts segregated from primitive magma with 120 ppm Cu, 0.04 ppb Ir, and 1 ppb Pd at various R factor values.

the harzburgites relative to the lherzolites and gabbros are because the former contains minor sulfides (Fig. 12B). Li et al. (2012) assumed that the parental magma of the Early Permian Kalatongke intrusion at the southern margin of the Central Asian orogenic belt contains ~1 ppb Pt, ~1 ppb Pd, and ~0.03 ppb Ir, whereas Song and Li (2009) proposed the PGE depletion resulted from prior sulfide removal. The PGE depletion of the Voisey's Bay parental magma (0.005 ppb Ir, 0.3 ppb Pt, 0.6 ppb Pd) was also attributed to retention of sulfide in the mantle source (Lightfoot et al., 2012).

Upgrading of sulfide and fractionation of sulfide melt

Experimental and empirical research has indicated that Os, Ir, Ru, and Rh tend to partition into MSS, whereas Pt, Pd, Au, and semimetals (Bi, Te, Sb and As) behave incompatibly and tend to concentrate in the residual Cu-rich sulfide liquid (e.g., Li et al., 1996; Mungall et al., 2005; Godel and Barnes, 2008; Helmy et al., 2010 and references therein). Relative to the sulfides of the No. 4 orebody, the sulfides of the No. 1 orebody and mineralized harzburgites are characterized by evidently high PGE concentrations and Se/S ratios as well as low Cu/Pd ratios and limited variation of δ^{34}S (Figs. 9–11). The positive correlation between Pd and Ir (Fig. 9C), decrease of the Ni/Ir ratios, and limited variation of the Pd/Ir ratios of the sparsely disseminated sulfides of the No. 1 orebody and mineralized harzburgites (Fig. 15) indicate that the sulfide liquids experienced upgrading of PGE by reaction with successive pulses of more primary S-unsaturated magma, rather than fractional crystallization of MSS (Lesher and Burnham, 2001). Such processing also resulted in elevation of the R factor, enrichment of metal elements, and decrease of Cu/Pd (Figs. 12, 14; e.g., Li et al., 2000, 2003; Lorand et al., 2003; Godel and Barnes, 2008; Song et al., 2008). In contrast, the negative correlation between Pd and Ir and the positive correlation between Ni/Ir and Pd/Ir of the disseminated sulfides of the No. 4 orebody again indicates the potential role of MSS fractional crystallization (Figs. 9C, 15). The fractionation of MSS has resulted in negative correlations of Ru versus Se, Te, and Bi in the No. 4 orebody, whereas no differentiation between Pt and the semimetal elements (Fig. 16), low PGE contents, high Cu/Pd ratios, and δ^{34}S values of the sulfides of the No. 4 orebody suggest extensive sulfide segregation due to more addition of crustal sulfur (Figs. 9–12B). An unavoidable problem is how the sulfide fractionation occurred in the disseminated sulfides containing only up to 20% sulfides in the No. 4 orebody.

The massive and net-textured sulfides containing more than 30% sulfides at the base of the northwestern part of the No. 4 orebody, as mentioned above, should have experienced fractional crystallization of MSS. When new pulses of magma containing unfractionated sulfide droplets entered the intrusion, the sulfide slurry containing early crystallized MSS may be disrupted. We believe that the disseminated sulfides of the No. 4 orebody are the product of reworking and mixing of the early sulfides and the new wave of magma containing unfractionated sulfide droplets. The mixture of the fractionated and unfractionated sulfides in variable proportions resulted in differentiation between IPGE and PPGE in the disseminated sulfides (Figs. 9C, 10). The previous net-textured and massive sulfides would be consumed gradually or even disappear.

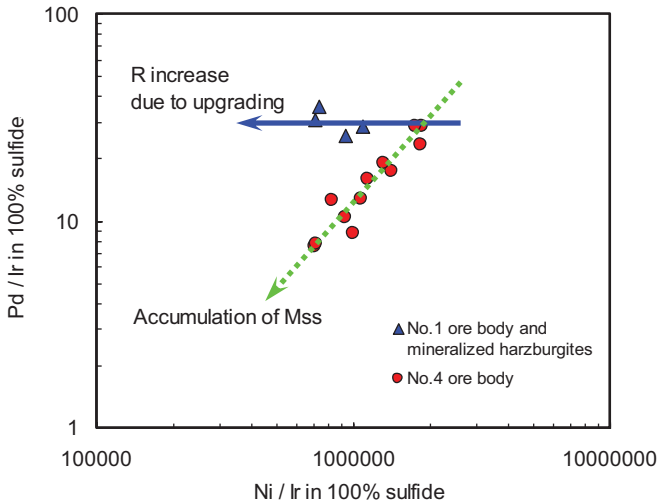

FIG. 15. Ratio plot of Pd/Ir vs. Ni/Ir of the Heishan sulfides, showing fractional crystallization of MSS (No. 4 orebody) and the PGE upgrade via reaction with fresh magma (No. 1 orebody and mineralized harzburgites; after Song et al., 2008).

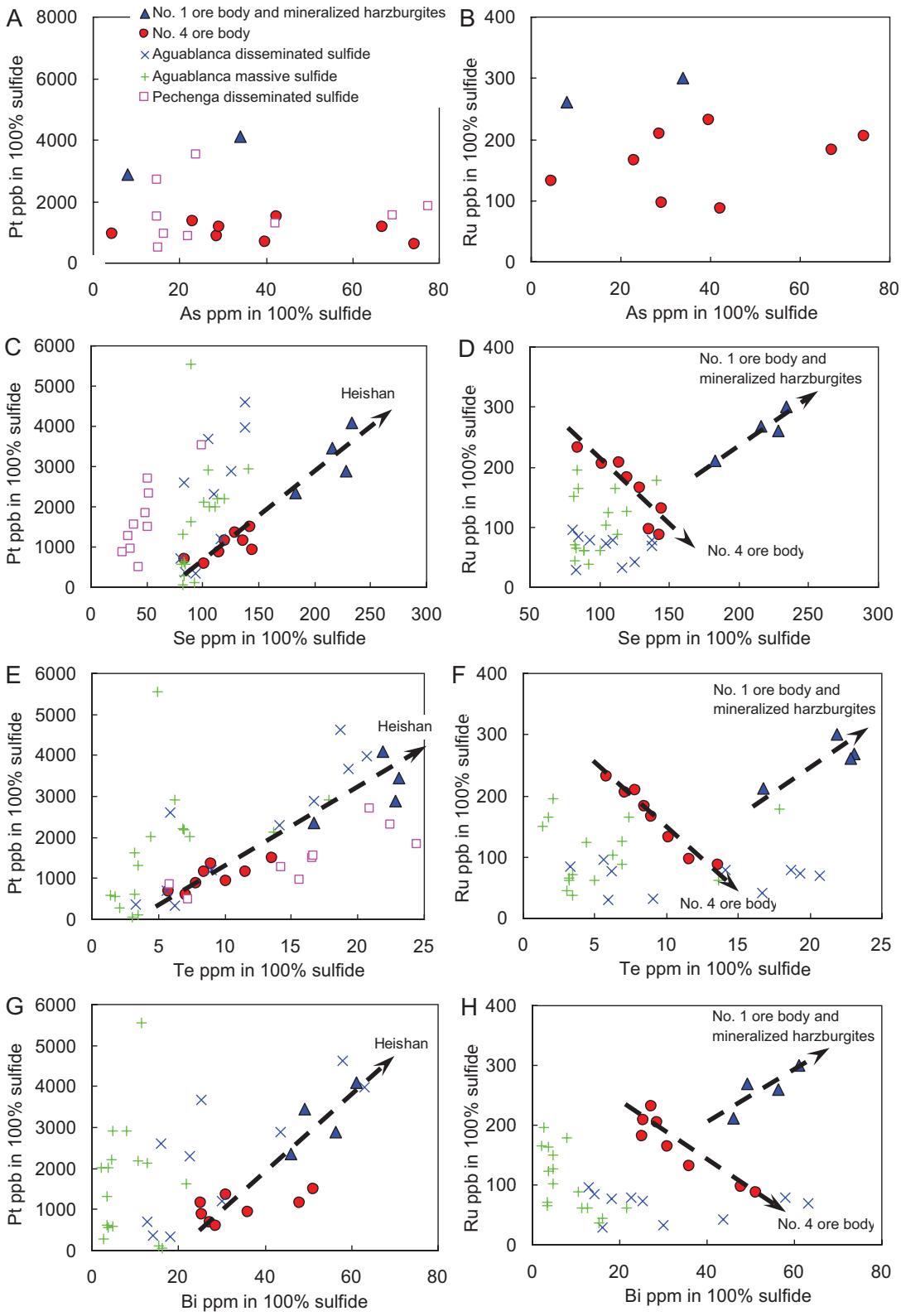

FIG. 16. Binary plots of platinum group and semimetal elements of the Heishan sulfides (No. 1 orebody and mineralized harzburgites ahd No. 4 orebody) on a 100% sulfide basis.

The formation of the disseminated sulfides in the leopard troctolite and varied-textured troctolite in the feeder sheet at Voisey's Bay, Canada, were attributed to a similar mechanism proposed by Li and Naldrett (1999), Naldrett et al. (2000), and Lightfoot et al. (2012).

Although it was recently proposed that most of the PGE (Ir, Rh, Pt ± Os, and Ru) formed sulfarsenide phases before or during the crystallization of MSS in the Creighton deposit, Sudbury (Dare et al., 2010a, b), the exsolution of PGE sulfarsenides from base metal sulfides is more common (Hanley, 2007; Barnes et al., 2008). Piña et al. (2008, 2012) proposed that small-sized tellurides and bismuthides in the disseminated sulfides of the Aguablanca Ni-Cu deposit (southwestern Spain) were formed by Pd, Pt, Te, and Bi exsolved from pyrrhotite and pentlandite as temperature decreased. On the other hand, Bi-Te phases, such as michenerite and tsumoite, are commonly formed and stable at late magmatic and/or hydrothermal stage (<540°C; Elliott, 1965; Hoffman and MacLean, 1976).

Similar to the disseminated sulfides of the Aguablanca and the Pechenga Ni-Cu deposits (Piña et al., 2008; Hanski et al., 2011), the disseminated sulfides of the Heishan No. 1 and No. 4 ore bodies show no correlation of As with Pt and Ru (Fig. 16A, B), positive correlations of Se, Te, and Bi with Pt (Fig. 16C, E, G), and negative correlations with Ru (Fig. 16D, F, H), indicating a fractional crystallization of MSS without PGM removal. On the other hand, the positive correlations of Se, Te, Bi, and Ru for the sulfides of the No. 1 orebody and the mineralized harzburgites are consistent with the reaction of the sulfide liquids with S-unsaturated magma (Fig. 16D, F, H). Although experimental work proposed that sperrylite may crystallize at high temperature ~1,400°C (Hansen and Anderko, 1958; Bennett and Heyding, 1966), saturation of arsenide and telluride in the sulfide melt requires at least ~0.1 wt % As and ~0.2 wt % Te, respectively (e.g., Makovicky et al., 1992; Fleet et al., 1993; Helmy et al., 2007). Very low contents of As, Te, and Bi and no discoveries of arsenide, telluride, and bismuthide in the Heishan sulfides probably suggest that these minerals did not reach saturation during fractionation of the sulfide liquids (Table 2).

Sulfide concentration in the Heishan intrusion

Magma conduits in magmatic plumbing systems are favorable sites for S-saturated magmas to form magmatic sulfide deposits (e.g., Naldrett, 1999, 2010; Arndt et al., 2005; Song et al., 2008, 2009b, 2012; Lightfoot et al., 2012 and references therein). The Heishan intrusion contains a very large proportion of ultramafic rock (>90%) and several reversals in olivine composition (Fig. 3), indicating that the intrusion was a staging magma chamber or a wider part of a plumbing system and that several pulses of magmas injected into the intrusion. Sr-Nd isotope values of the intrusive rocks and wall rocks at Heishan are consistent with the crustal contamination at depth (Xie et al., 2012) as the wall rocks are barren of sulfide. This model requires that the crustal sulfur addition and sulfide segregation occurred at depth.

We propose when the magma containing sulfide droplets entered the Heishan intrusion, the sulfide droplets and olivine and pyroxene settled down because of decrease of the flow velocity of the magma. Sulfide liquid accumulated at the entry of the intrusion formed the massive and net-textured sulfides, which experienced fractional crystallization of MSS in the drill hole ZK803. When new pulses of magma containing unfractionated sulfide droplets entered the intrusion, the MSS slurry may have been disrupted and mixed with the unfractionated sulfide droplets in variable proportions and deposited at the base of the intrusion to form the disseminated sulfides of the No. 4 orebody. We infer that a magma feeder conduit probably is close to drill hole ZK 803 at the northwestern part of the Heishan intrusion. On the other hand, the sulfide droplets remaining in the deep-seated staging magma chamber were upgraded in PGE by reaction with new S-unsaturated magma and were carried to the Heishan intrusion later to form the No. 1 orebody and the mineralized harzburgites in higher levels of the intrusion.

Conclusions

The Late Devonian Heishan magmatic Ni-Cu-(PGE) deposit was formed in a magma plumbing system at an active continental margin. The associated magmas were generated by partial melting of mantle wedge and uprising asthenosphere that were originally Cu-enriched and weakly PGE-depleted. The sulfides of the No. 4 orebody were formed by settling of the mixtures of unfractionated sulfide liquids and previously fractionated MSS slurry at the base of the intrusion. The sulfide segregation was triggered by addition of crustal sulfur during contamination at a deep-seated magma chamber. Whereas, the sulfides upgraded in chalcophile elements by reaction of the sulfide droplets with the new pulses of S-unsaturated magma in the deep-seated magma chamber were brought to the Heishan intrusion and formed the No. 1 orebody and the mineralized harzburgites in higher levels.

Acknowledgments

This study was funded by the CAS/SAFEA International Partnership Program for Creative Research Teams (Intraplate Mineralization Research Team; KZZD-EW-TZ-20) and research grants from State Key Laboratory of Ore Deposit Geochemistry (SKLODG-ZY125-06) and NSFC (41172090 and 40973038) to Xie-Yan Song and NSFC (41003022) to Lie-Meng Chen. We are grateful to Yu-Long Tian, Bo Ma, Chao-Bo Zhang, and Jun-Zhen Yu for their support in our field work. We benefited from discussion with Chusi Li and Tony Naldrett. At last, we are grateful to associate editor Steve Barnes and reviewer Peter Lightfoot for their constructive comments and suggestions to our manuscript.

REFERENCES

Arndt, N., Lesher, C.M., and Czamanske, G.K., 2005, Mantle-derived magmas and magmatic Ni-Cu-(PGE) deposits: Economic Geology, v. 100, p. 5–24.

Barnes, S.J., and Liu, W., 2012, Pt and Pd mobility in hydrothermal fluids: evidence from komatiites and from thermodynamic modeling: Ore Geology Reviews, v. 44, p. 49–58.

Barnes, S.J., and Naldrett, A.J., 1985, Geochemistry of the J-M (Howland) Reef of the Stillwater Complex, Minneapolis Adit area, I. Sulfide chemistry and sulfide-olivine equilibrium: Economic Geology, v. 80, p. 627–645.

Barnes, S.J., Wells, M.A., and Verrall, M.R., 2009, Effects of magmatic processes, serpentinization, and talc carbonate alteration on sulfide mineralogy and ore textures in the Black Swan disseminated nickel sulfide deposit, Yilgarn craton: Economic Geology, v. 104, p. 539–562.

Barnes, S.J., Osborne, G.A., Cook, D., Barnes, L., Maier, W.D., and Godel, B., 2011, The Santa Rita nickel sulfide deposit in the Fazenda Mirabela intrusion, Bahia, Brazil: Geology, sulfide geochemistry, and genesis: Economic Geology, v. 106, p. 1083–1110.

Barnes, S.J., Godel, B., Gürer, D., Brenan, J.M., Robertson, J., and Paterson, D., 2013, Sulfide-olivine Fe-Ni exchange and the origin of anomalously Ni rich magmatic sulfides: Economic Geology, v. 108, p. 1971–1982.

Barnes, S.-J., and Lightfoot, P.C., 2005, Formation of magmatic nickel sulfide ore deposits and processes affecting their copper and platinum group element contents: Economic Geology 100th Anniversary Volume, p. 179–213.

Barnes, S.-J., and Maier, W.D., 1999, The fractionation of Ni, Cu and the noble metals in silicate and sulphide liquids, *in* Keays, R.R., Lesher, C.M., Lightfoot, P.C., and Farrow, C.E.G., eds., Dynamic processes in magmatic ore deposits and their application to mineral exploration, Geological Association of Canada, Short Course Notes, p. 69–106.

Barnes, S.-J., Boyd, R., Korneliussen, A., Nilsson, L.-P., Often, M., Pedersen, R.B., and Robins, B., 1988, The use of mantle normalization and metal ratios in discriminating between the effects of partial melting, crustal fractionation and sulphide segregation on platinum group elements, gold, nickel and copper: Examples from Norway, *in* Prichard, H.M, Potts, P.J., Bowles, J.F.W., and Cribbs, S.J., eds., Geoplatinum-87: London, Elsevier, Applied Science, p. 113–143.

Barnes, S.-J., Couture, J.F., Sawyer, E.W., and Bouchaib, C., 1993, Nickel-copper occurrences in the Belleterre-Angliers belt of the Pontiac subprovince and the use of Cu-Pd ratios in interpreting platinum-group element distributions: Economic Geology, v. 88, p. 1402–1418.

Barnes, S.-J., Zientek, M.L., and Severson, M.J., 1997, Ni, Cu, Au, and platinum-group element contents of sulphides associated with intraplate magmatism: A synthesis: Canadian Journal of Earth Sciences, v. 34, p. 337–351.

Barnes, S.-J., Prichard, H.M., Cox, R.A., Fisher, P.C., and Godel, B., 2008, The location of the chalcophile and siderophile elements in platinum-group element ore deposits (a textural, microbeam and whole rock geochemical study): Implications for the formation of the deposits: Chemical Geology, v. 248, p. 295–317.

Begg, G.C., Hronsky, J.A.M., Arndt, N.T., Griffin, W.L., O'Reilly, S.Y., and Hayward, N., 2010, Lithospheric, cratonic, and geodynamic setting of Ni-Cu-PGE sulfide deposits: Economic Geology, v. 105, p. 1057–1070.

Bennet, S.L., and Heyding, R.D., 1966, Arsenides of the transition metals. VIII. Some binary and ternary group VIII diarsenides and their magnetic and electrical properties: Canadian Journal of Chemistry, v. 44, p. 3017–3030.

Bezmen, N.S., Asif, M., Brugmann, G.E., Romanenko, I.M., and Naldrett, A.J., 1994, Experimental determinations of sulfide-silicate partitioning of PGE and Au: Geochimica et Cosmochimica Acta, v. 58, p. 1251–1260.

BGMRG (Bureau of Geology and Mineral Resources of Gansu Province), 1989, Regional geology of Gansu province: Geological Memoirs 19, Beijing, Geological Publishing House (in Chinese).

BGMRXUAR (Bureau of Geology and Mineral Resources of Xinjiang Uygur Autonomous Region), 1993, Regional geology of Xinjiang autonomous region: Geological Memoirs 32, Beijing, Geological Publishing House (in Chinese).

Botcharnikov, R.E., Linnen, R.L., Wilke, M., Holtz, F., Jugo, P.J., and Berndt, J., 2010, High gold concentrations in sulphide-bearing magma under oxidizing conditions: Nature Geoscience, v. 4, p. 112–115.

Brandon, A.D., Creaser, R.A., Shirey, S.B., and Carlson, R.W., 1996, Os recycling in subduction zones: Science, v. 272, p. 861–864.

Brenan, J.M., and Caciagli, N.C., 2000, Fe-Ni exchange between olivine and sulphide liquid: Implications for oxygen barometry in sulphide-saturated magmas: Geochimica et Cosmochimica Acta, v. 64, p. 307–320.

Campbell, I.H., and Barnes, S.J., 1984, A model for the geochemistry of the platinum group elements in magmatic sulphide deposits: Canadian Mineralogist, v. 22, p. 151–160.

Campbell, I.H., and Naldrett, A.J., 1979, The influence of silicate:sulfide ratios on the geochemistry of magmatic sulfides: Economic Geology, v. 74, p. 1503–1506.

Casquet, C., Galindo, C., Tornos, F., Velasco, F., and Canales, A., 2001, The Aguablanca Cu-Ni ore deposit (Extremadura, Spain): A case of synorogenic orthomagmatic mineralization: Age and isotope composition of magmas (Sr, Nd) and ore (S): Ore Geology Reviews, v. 18, p. 237–250.

Charvet, J., Shu, L., and Laurent-Charvet, S., 2007, Paleozoic structural and geodynamic evolution of eastern Tianshan (NW China): Welding of the Tarim and Junggar plates: Episodes, v. 30, p. 162–185.

Chen, C.M., Lu, H.F., Jia, D., Cai, D.S., and Wu, S.M., 1999, Closing history of the southern Tianshan oceanic basin, western China: An oblique collisional orogeny: Tectonophysics, v. 302, p. 23–40.

Chen, L.-M., Song, X.-Y., Keays, R.R., Tian, Y.-L., Wang, Y.-S., Deng, Y.-F., and Xiao, J.-F., 2013, Segregation and fractionation of magmatic Ni-Cu-PGE sulfides in the western Jinchuan intrusion, northwestern China: Insights from platinum group element geochemistry: Economic Geology, v. 108, p. 1793–1811.

Crocket, J.H., 2002, Platinum-group element geochemistry of mafic and ultramafic rocks: Canadian Institute of Mining, Metallurgy and Petroleum Special Volume 54, p. 177–210.

Crocket, J.H., Fleet, M.E., and Stone, W.E., 1997, Implications of composition for experimental partitioning of platinum-group elements and gold between sulfide liquid and basalt melt: The significance of nickel: Geochimica et Cosmochimica Acta, v. 61, p. 4139–4149.

Czamanske, G.K., Kunilov, V.E., Zientek, M.L., Cabri, L.J., Likhachev, A.P., Calk, L.C., and Oscarson, R.L., 1992, A proton-microprobe study of magmatic sulphide ores from the Noril'sk-Talnakh district, Siberia: Canadian Mineralogist, v. 30, p. 249–287.

Dare, S.A.S., Barnes, S.-J., Prichard, H.M., and Fisher, P.C., 2010a, The timing and formation of platinum-group minerals from the Creighton Ni-Cu-platinum-group element sulfide deposit, Sudbury, Canada: Early crystallization of PGE-rich sulfarsenides: Economic Geology, v. 105, p. 1071–1096.

Dare, S.A.S., Barnes, S.-J., and Prichard, H.M., 2010b, The distribution of platinum group elements and other chalcophile elements among sulfides from the Creighton Ni-Cu-PGE sulfide deposit, Sudbury, Canada, and the origin of Pd in pentlandite: Mineralium Deposita, v. 45, p. 765–793.

Deng, Y.-F., Song, X.-Y., Chen, L.-M., Zhou, T., Pirajno, F., Yuan, F., Xie, W., and Zhang, D., 2014, Geochemistry of the Huangshandong Ni-Cu deposit in northwestern China: Implications for the formation of magmatic sulfide mineralization in orogenic belts: Ore Geology Reviews, v. 56, p. 181–198.

Ebel, D.S., and Naldrett, A.J., 1996, Fractional crystallization of sulfide ore liquids at high temperature: Economic Geology, v. 91, p. 607–621.

Eckstrand, O.R., Grinenko, L.N., Krouse, H.R., Paktunc, A.D., Schwann, P.L., and Scoates, R.F.J., 1989, Preliminary data on sulphur isotopes and Se/S ratios, and the source of sulphur in magmatic sulphides from the Fox River sill, Molson dykes, and Thompson nickel deposits, northern Manitoba: Geological Survey of Canada Paper 89-1C, p. 235–242.

Elliott, R.P., 1965, Constitution of binary alloys, 1st supplement: Materials Science and Engineering Series, New York, McGraw-Hill, 877 p.

Evans, K.A., Elburg, M.A., and Kamenetsky, V.S., 2012, Oxidation state of subarc mantle: Geology, v. 40, p. 783–786.

Fiorentini, M.L., Barnes, S.J., Lesher, C.M., Heggie, G.J., Keays, R.R., and Burnham, O.M., 2010, Platinum group element geochemistry of mineralized and nonmineralized komatiites and basalts: Economic Geology, v. 105, p. 795–823.

Fleet, M.E., Chryssoulis, S.L., Stone, W.E., and Weisener, C.G., 1993, Partitioning of platinum group elements and Au in the Fe-Ni-Cu-S system: Experiments on the fractional crystallization of sulphide melt: Contributions to Mineralogy and Petrology, v. 115, p. 36–44.

Gao, J.-F., Zhou, M.-F., Lightfoot, P.C., Wang, C.Y., and Qi, L., 2012, Origin of PGE-poor and Cu-rich magmatic sulfides from the Kalatongke deposit, Xinjiang, northwest China: Economic Geology, v. 107, p. 481–506.

Gao, J.-F., Zhou, M.-F., Lightfoot, P.C., Wang, C.Y., Qi, L., and Sun, M., 2013, Sulfide saturation and magma emplacement in the formation of the Permian Huangshandong Ni-Cu sulfide deposit, Xinjiang, northwestern China: Economic Geology, v. 108, p. 1833–1848.

Ge, R., Zhu, W., Wu, H., Zheng, B., Zhu, X., and He, J., 2012, The Paleozoic northern margin of the Tarim craton: Passive or active?: Lithos, v. 142-143, p. 1–15.

Godel, B., and Barnes, S.-J., 2008, Platinum-group elements in sulfide minerals and the whole rocks of the J-M Reef (Stillwater Complex): Implication for the formation of the reef: Chemical Geology, v. 248, p. 272–294.

Govindaraju, K., 1994, Compilation of working values and sample description for 383 geostandards: Geostandards and Geoanalytical Research, v. 18, p. 1–158.

Han, B.F., Ji, J.Q., Song, B., Chen, L.H., and Li, Z.H., 2004, Zircon SHRIMP U-Pb age and geology of Kalatongke-Huangshan mafic-ultramafic complex, Xinjiang, China: Chinese Science Bulletin, v. 49, p. 2324–2328 (in Chinese with English abs.).

Han, B.F., He, G.Q., Wang, X.C., and Guo, Z.J., 2011, Late Carboniferous collision between the Tarim and Kazakhstan-Yili terranes in the western segment

of the South Tian Shan orogen, Central Asia, and implications for the northern Xinjiang, western China: Earth-Science Reviews, v. 109, p. 74–93.

Hansen, M., and Anderko, K., 1958, Constitution of binary alloys: New-York, McGraw-Hill, Schenectady, New York, General Electric Co., Business Growth Services, 1,305 p.

Hanski, E.J., Luo, Z.-Y., Oduro, H., and Walker, R.J., 2011, The Pechenga Ni-Cu sulfide deposits, northwestern Russia: A review with new constraints from the feeder dikes: Economic Geology, v. 17, p. 145–162.

Heinrich, C.A., Günther, D., Audétat, A., Ulrich, T., and Frischknecht, R., 1999, Metal fractionation between magmatic brine and vapor, determined by microanalysis of fluid inclusions: Geology, v. 27, p. 755–758.

Helmy, H.M., Ballhaus, C., Berndt, J., Bockrath, C., and Wohlgemuth-Ueerwasser, C., 2007, Formation of Pt, Pd and Ni tellurides: Experiments in sulphide-telluride systems: Contribution to Mineralogy and Petrology, v. 153, p. 577–591.

Helmy, H.M., Ballhaus, C., Wohlgemuth-Ueerwasser, C., Fonseca, R.O.C., and Laurenz, V., 2010, Partitioning of Se, As, Sb, Te and Bi between monosulfide solid solution and sulfide melt—application to magmatic sulfide deposits: Geochimica et Cosmochimica Acta, v. 74, p. 6174–6179.

Hoffman, E.L., and MacLean, W.H., 1976, Phase relations of michenerite and merenskyite in the Pd-Bi-Te system: Economic Geology, v. 71, p. 1461–1468.

Hu, A.Q., Jahn, B.M., Zhang, G., Chen, Y., and Zhang, Q., 2000, Crustal evolution and Phanerozoic crustal growth in northern Xinjiang: Nd isotopic evidence. Part I. Isotopic characterization of basement rocks: Tectonophysics, v. 328, p. 15–51.

Jahn, B., Windley, B., Natal'in, B., and Dobretsov, N., 2004, Phanerozoic continental growth in Central Asia: Journal of Asian Earth Sciences, v. 23, p. 599–603.

Jiao, J.G., Tang, Z.L., Qian, Z.Z., Duan, j., and Jiang, C., 2012, Genesis and metallogenic process of Tulargen large scale Cu-Ni sulfide deposit in eastern Tianshan area, Xinjiang: Acta Petrologica Sinica, v. 28, p. 3772–3786 (in Chinese with English abs.).

Jiao, J.G., Zheng, P.P., Liu, R.P., Duan, J., and Jiang, C., 2013, SHRIMP zircon U-Pb of the No. 3 intrusion in the Tulargen Cu-Ni mining area, East Tianshan Mountains, Xinjiang, and its Geological Significance: Geology and Exploration, v. 49, p. 393–404 (in Chinese with English abs.).

Keays, R.R., 1995, The role of komatiitic and picritic magmatism and S-saturation in the formation of ore deposits: Lithos, v. 34, p. 1–18.

Keays, R.R., and Jowitt, S.M., 2013, The Avebury Ni deposit, Tasmania: A case study of an unconventional nickel deposit: Ore Geology Reviews, v. 52, p. 4–17.

Keays, R.R., and Lightfoot, P.C., 2007, Siderophile and chalcophile metal variations in Tertiary picrites and basalts from West Greenland with implications for the sulphide saturation history of continental flood basalt magmas: Mineralium Deposita, v. 42, p. 319–336.

Lesher, C.M., and Burnham, O.M., 2001, Multicomponent elemental and isotopic mixing in Ni-Cu- (PGE) ores at Kambalda, Western Australia: Canadian Mineralogist, v. 39, p. 421–446.

Li, C., and Naldrett, A.J., 1999, Geology and petrology of the Voisey's Bay intrusion: Reaction of olivine with sulfide and silicate liquids: Lithos, v. 47, p. 1–31.

Li, C., Barnes, S.-J., Makovicky, E., Rose-Hansen, J., and Makovicky, M., 1996, Partitioning of nickel, copper, iridium, rhenium, platinum, and palladium between monosulfide solid solution and sulfide liquid: Effects of composition and temperature: Geochimica et Cosmochimica Acta, v. 60, p. 1231–1238.

Li, C., Lightfoot, P.C., Amelin, Y., and Naldrett, A.J., 2000, Contrasting petrological and geochemical relationships in the Voisey's Bay and Mushuau intrusions, Labrador, Canada: Implications for ore genesis: Economic Geology, v. 95, p. 771–799.

Li, C., Ripley, E.M., and Naldrett, A.J., 2003, Compositional variations of olivine and sulfur isotopes in the Noril'sk and Talnakh intrusions, Siberia: Implications for ore-forming processes in dynamic magma conduits: Economic Geology, v. 98, p. 69–86.

Li, C., Zhang, M., Fu, P., Qian, Z., Hu, P., and Ripley, E.M., 2012, The Kalatongke magmatic Ni-Cu deposits in the Central Asian orogenic belt, NW China: Product of slab window magmatism?: Mineralium Deposita, v. 47, p. 51–67.

Lightfoot, P.C., Keays, R.R., Evans-Lamswood, D., and Wheeler, R., 2012, S saturation history of Nain Plutonic Suite mafic intrusions: Origin of the Voisey's Bay Ni-Cu-Co sulfide deposit, Labrador, Canada: Mineralium Deposita, v. 47, p. 23–50.

Liu, X.C., Chen, B.L., Jahn, B., Wu, G.G., and Liu, Y.S., 2011, Early Paleozoic (ca. 465 Ma) eclogites from Beishan (NW China) and their bearing on the tectonic evolution of the southern Central Asian orogenic belt: Journal of Asian Earth Sciences, v. 42, p. 715–731.

Lorand, J.-P., Alard, O., Luguet, A., and Keays, R.R., 2003, Sulfur and selenium systematics of the subcontinental lithosperic mantle: Inferences from the Massif Central xenolith suite (France): Geochimica et Cosmochimica Acta, v. 67, p. 4137–4151.

Makovicky, M., Makovicky, E., and Rose-Hansen, J., 1992, The phase system Pt-Fe-As-S at 850°C and 470°C: Neues Jahrbuch für Mineralogie Monatshefte, v. 10, p. 441–453.

Maier, W.D., and Groves, D.I., 2011, Temporal and spatial controls on the formation of magmatic PGE and Ni-Cu deposits: Mineralium Deposita, v. 46, p. 841–857.

Maier, W.D., Barnes, S.-J., Chinyepi, G., Barton Jr, J.M., Eglington, B., and Setshedi, I., 2008, The composition of magmatic Ni-Cu-(PGE) sulfide deposits in the Tati and Selebi-Phikwe belts of eastern Botswana: Mineralium Deposita, v. 43, p. 37–60.

Mao, J.W., Pirajno, F., Zhang, Z.H., Chai, F.M., Wu, H., Chen, S.P., Cheng, S.L., Yang, J.M., and Zhang, C.Q., 2008, A review of the Cu-Ni sulphide deposits in the Chinese Tianshan and Altay orogens (Xinjiang autonomous region, NW China): Principal characteristics and ore-forming processes: Journal of Asian Earth Sciences, v. 32, p. 184–203.

McDonough, W.F., and Sun, S.-s., 1995, The composition of the Earth: Chemical Geology, v. 120, p. 223–253.

McInnes, B.I.A., McBride, J.S., Evans, N.J., Lambert, D.D., and Andrew, A.S., 1999, Osmium isotope constraint on ore metal recycling in subduction zones: Science, v. 286, p. 512–516.

Mungall, J.E., Andrews, D.R.A., Cabri, L.J., Sylvester, P.J., and Tubrett, M., 2005, Partitioning of Cu, Ni, Au, and platinum-group elements between monosulfide solid solution and sulfide melt under controlled oxygen and sulfur fugacities: Geochimica et Cosmochimica Acta, v. 69, p. 4349–4360.

Naldrett, A.J., 1999, World-class Ni-Cu-PGE deposits: Key factors in their genesis: Mineralium Deposita, v. 34, p. 227–240.

——2004, Magmatic sulfide deposits: Geology, geochemistry and exploration: Springer, 727 p.

——2010, From the mantle to the bank: the life of a Ni-Cu-(PGE) sulfide deposit: South African Journal of Geology, v. 113, p. 1–32.

Naldrett, A.J., and Barnes, S.-J., 1986, The behavior of platinum group elements during fractional crystallization and partial melting with special reference to the composition of magmatic sulfide ores: Fortschritte Mineralogie, v. 64, p. 113–133.

Naldrett, A.J., Innes, D.C., Sowa, J., and Gorton, M.P., 1982, Compositional variations within and between five Sudbury ore deposits: Economic Geology, v. 77, p. 1519–1534.

Naldrett, A.J., Asif, M., Krstic, S., and Li, C., 2000, The composition of mineralization at the Voisey's Bay Ni-Cu sulfide deposit, with special reference to platinum-group elements: Economic Geology, v. 95, p. 845–865.

Paktunc, A.D., Hulbert, L.J., and Harris, D.C., 1990, Partitioning of the platinum-group and other trace elements in sulfides from the Bushveld Complex and Canadian occurrences of nickel-copper sulfides: Canadian Mineralogist, v. 28, p. 475–488.

Peach, C.L., Mathez, E.A., and Keays, R.R., 1990, Sulfide melt-silicate melt distribution coefficients for noble metals and other chalcophile elements as deduced from MORB: Implications for partial melting: Geochimica et Cosmochimica Acta, v. 54, p. 3379–3389.

Peltonen, P., 1995, Magma-country rock interaction and the genesis of Ni-Cu deposits in the Vammala nickel belt, SW Finland: Mineralogy and Petrology, v. 52, p. 1–24.

Piña, R., Lunar, R., Ortega, L., Gevilla, F., Alapieti, T., and Martínez, C., 2006, Petrology and geochemistry of mafic-ultramafic fragments from the Aguablanca Ni-Cu ore breccia, southwest Spain: Economic Geology, v. 101, p. 865–881.

Piña, R., Gervilla, F., Ortega, L., and Lunar, R., 2008, Mineralogy and geochemistry of platinum-group elements in the Aguablanca Ni-Cu deposit (SW Spain): Mineralogy and Petrology, v. 92, p. 259–282.

Piña, R., Gervilla, F., Barnes, S.-J., Ortega, L., and Lunar, R., 2012, Distribution of platinum-group and chalcophile elements in the Aguablanca Ni-Cu sulfide deposit (SW Spain): Evidence from a LA-ICP-MS study: Chemical Geology, v. 302–303, p. 61–75.

Puchtel, I.S., and Humayun, M., 2001, Platinum group element fractionation in a komatiitic basalt lava lake: Geochimica et Cosmochimica Acta, v. 65, p. 2979–2993.

Qi, L., Zhou, M.-F., and Wang, C.Y., 2004, Determination of low concentrations of platinum group elements in geological samples by ID-ICP-MS: Journal of Analytical Atomic Spectrometry, v. 19, p. 1335–1339.

Qi, L., Zhou, M.-F., Wang, C.Y., and Sun, M., 2007, Evaluation of the determination of Re and PGEs abundances of geological samples by ICP-MS coupled with a modified Carius tube digestion at different temperatures: Geochemical Journal, v. 41, p. 407–414.

Qin, K., Su, B., Sakyi, P.A., Tang, D., Li, X., Sun, H., Xiao, Q., and Liu, P., 2011, SIMS zircon U-Pb geochronology and Sr-Nd isotopes of Ni-Cu-bearing mafic-ultramafic intrusions in Eastern Thanshan and Beishan in correlation with flood basalts in Tarim basin (NW China): Constraints on a ca. 280 Ma mantle plume: American Journal of Science, v. 311, p. 237–260.

Queffurus, M., and Barnes, S.-J., in press, Processes affecting the sulfur to selenium ratio in magmatic nickel-copper and platinum-group element deposits: Ore Geology Reviews.

Rehkämper, M., Halliday, A.N., Barfod, D., Fitton, J.G., and Dawson, G.J., 1997, Platinum-group element abundance patterns in different mantle environments: Science, v. 278, p. 1595–1598.

Righter, K., Campbell, A.J., Humayun, M., and Hervig, R.L., 2004, Partitioning of Ru, Rh, Pd, Re, Ir, and Au between Cr-bearing spinel, olivine, pyroxene and silicate melts: Geochimica et Cosmochimica Acta, v. 68, p. 867–880.

Ripley, E.M., and Li, C., 2003, Sulfur isotope exchange and metal enrichment in the formation of magmatic Cu-Ni-(PGE) deposits: Economic Geology, v. 98, p. 635–641.

Ripley, E.M., Brophy, J.G., and Li, C., 2002, Copper solubility in a basaltic melt and sulfide liquid/silicate melt partition coefficients of Cu and Fe: Geochimica et Cosmochimica Acta, v. 66, p. 2791–2800.

San, J.Z., Qin, K.Z., Tang, Z.L., Tang, D.M., Su, B.X., Sun, H., Xiao, Q.H., and Liu, P.P., 2010, Precise zircon U-Pb age dating of two mafic-ultramafic complexes at Tulargen large Cu-Ni district and its geological implications: Acta Petrologica Sinica, v. 26, p. 3027–3035 (in Chinese with English abs.).

Sattari, P., Brenan, J.M., Horn, I., and McDonough, W.F., 2002, Experimental constraints on the sulfide- and chromite-silicate melt partitioning behavior of rhenium and platinum group elements: Economic Geology, v. 97, p. 385–398.

Seat, Z., Beresford, S.W., Grguric, B.A., Gee, M.A.M, and Grassineau, N.V., 2009, Reevaluation of the role of external sulfur addition in the genesis of Ni-Cu-PGE deposits: Evidence from the Nebo-Babel Ni-Cu-PGE deposit, West Musgrave, Western Australia: Economic Geology, v. 104, p. 521–538.

Seat, Z., Gee, M.A.M, Grguric, B.A., Beresford, S.W., and Grassineau, N.V., 2011, The Nebo-Babel Ni-Cu-PGE sulfide deposit (West Musgrave, Australia): Pt. 1. U/Pb zircon ages, whole-rock and mineral chemistry, and O-Sr-Nd isotope compositions of the intrusion, with constraints on petrogenesis: Economic Geology, v. 106, p. 527–556.

Seedorff, E., Dilles, J.H., Proffett Jr, J.M., and Einaudi, M.T., 2005, Porphyry deposits: Characteristics and origin of hypogene features: Economic Geology 100th Anniversary Volume, p. 251–298.

Sengör, A.M.C., Natal'In, B.A., and Burtman, V.S., 1993, Evolution of the Altaid tectonic collage and Palaeozoic crustal growth in Eurasia: Nature, v. 364, p. 299–307.

Song, X.-Y., and Li, X.-R., 2009, Geochemistry of the Kalatongke Ni-Cu-(PGE) sulfide deposit, NW China: Implications for the formation of magmatic sulfide mineralization in a postcollisional environment: Mineralium Deposita, v. 44, p. 303–327.

Song, X.-Y., Zhou, M.-F., Wang, C.Y., and Qi, L., 2006, Role of crustal contamination in formation of the Jinchuan intrusion and its world-class Ni-Cu-(PGE) sulfide deposit, NW China: International Geological Review, v. 48, p. 1113–1132.

Song X.-Y., Zhou, M.-F., Tao, Y., and Xiao, J.-F., 2008, Controls on the metal compositions of magmatic sulfide deposits in the Emeishan large igneous province, SW China: Chemical Geology, v. 253, p. 38–49.

Song, X.-Y., Keays, R.R., Xiao, L., Qi, H.-W., and Ihlenfeld, C., 2009a, Platinum-group element geochemistry of the continental flood basalts in the certral Emeishan large igneous province, SW China: Chemical Geology, v. 262, p. 246–261.

Song, X.-Y., Keays, R.R., Zhou, M.-F., Qi, L., Ihlenfeld, C., and Xiao, J.-F., 2009b, Siderophile and chalcophile elemental constraints on the origin of the Jinchuan Ni-Cu-(PGE) sulfide deposit, NW China: Geochimica et Cosmochimica Acta, v. 73, p. 404–424.

Song, X.-Y., Xie, W., Deng, Y.-F., Crawford, A.J., Zheng, W.-Q., Zhou, G.-F., Deng, G., Cheng, S.-L., and Li, J., 2011, Slab break-off and the formation of Permian mafic-ultramafic intrusions in southern margin of Central Asian orogenic belt, Xinjiang, NW China: Lithos, v. 127, p. 128–143.

Song, X.-Y., Danyushevsky, L.V., Keays, R.R., Chen, L.-M., Wang, Y.-S., Tian, Y.-L., and Xiao, J.-F., 2012, Structural, lithological, and geochemical constraints on the dynamic magma plumbing system of the Jinchuan Ni-Cu sulfide deposit, NW China: Mineralium Deposita, v. 47, p. 277–297.

Song, X.-Y., Chen, L.-M., Deng, Y.-F., and Xie, W., 2013, Syn-collisional tholeiitic magmatism induced by slab detachment at the southern margin of the Central Asian orogenic belt: Journal of the Geological Society, v. 170, p. 941–950.

Stone, W.E., Crocket, J.H., and Fleet, M.E., 1990, Partitioning of palladium, iridium, platinum and gold between sulfide liquid and basalt melt at 1200°C: Geochimica et Cosmochimica Acta, v. 54, p. 2341–2344.

Sun, T., Qian, Z.-Z., Deng, Y.-F., Li, C., Song, X.-Y., and Tang, Q., 2013, PGE and isotope (Hf-Sr-Nd-Pb) constraints on the origin of the Huangshandong magmatic Ni-Cu sulfide deposit in the Central Asian orogenic belt, northwestern China: Economic Geology, v. 108, p. 1849–1864.

Sun, W., Zhang, H., Ling, M.-X., Ding, X., Chung, S.-L., Zhou, J., Yang, X.-Y., and Fan, W., 2011, The genetic association of adakites and Cu-Au ore deposits: International Geology Review, v. 53, p. 691–703.

Tang, D., Qin, K., Li, C., Qi, L., Su, B., and Qu, W., 2011, Zircon dating, Hf-Sr-Nd-Os isotopes and PGE geochemistry of the Tianyu sulfide-bearing mafic-ultramafic intrusion in the Central Asian orogenic belt, NW China: Lithos, v. 126, p. 84–98.

Thakurta, J., Ripley, E.M., and Li, C., 2008, Geochemical constraints on the origin of sulfide mineralization in the Duke Island Complex, southeastern Alaska: Geochemistry Geophysics Geosystems, v. 9, Q07003, doi:10.1029/2008GC001982.

Thériault, R.D., and Barnes, S.-J., 1998, Compositional variations in Cu-Ni-PGE sulfides of the Dunka Road deposit, Duluth Complex, Minnesota: The importance of combined assimilation and magmatic processes: Canadian Mineralogist, v. 36, p. 869–886.

Wang, J., and Xu, X., 2006, Post-collisional tectonic evolution and metallogenesis in northern Xinjiang, China: Acta Geologica Sinica, v. 80, p. 24–31 (in Chinese with English abs.).

Windley, B.F., Alexeiev, D., Xiao, W., Kröner, A., and Badarch, G., 2007, Tectonic models for accretion of the Central Asian orogenic belt: Journal of Geological Society, v. 164, p. 31–47.

Woodland, S.J., Pearson, D.G., and Thirlwall, M.F., 2002, A platinum group element and Re-Os isotope investigation of siderophile element recycling in subduction zones: Comparison of Grenada, Lesser Antilles arc, and the Izu-Bonin arc: Journal of Petrology, v. 43, p. 171–198.

Xia, M.-Z., Jiang, C.-Y., Li, C., and Xia, Z.-D., 2013, Characteristics of a newly discovered Ni-Cu sulfide deposit hosted in the Poyi ultramafic intrusion, Tarim craton, NW China: Economic Geology, v. 108, p. 1865–1878.

Xiao, W.-J., Zhang, L.-C., Qin, K.-Z., Sun, S., and Li, J.-L., 2004, Paleozoic accretionary and collisional tectonics of the eastern Tianshan (China): Implications for the continental growth of Central Asia: American Journal of Science, v. 304, p. 370–395.

Xiao, W., Han, C., Yuan, C., Sun, M., Lin, S., Chen, H., Li, Z., Li, J., and Sun, S., 2008, Middle Cambrian to Permian subduction-related accretionary orogenesis of northern Xinjiang, NW China: Implications for the tectonic evolution of Central Asia: Journal of Asian Earth Sciences, v. 32, p. 102–117.

Xiao, W.J., Mao, Q.G., Windley, B.F., Han, C.M., Qu, J.F., Zhang, J.E., Ao, S.J., Guo, Q.Q., Ckeven, N.R., Lin, S.F., Shan, Y.H., and Li, J.L., 2010, Paleozoic multiple accretionary and collisional processes of the Beishan orogenic collage: American Journal of Science, v. 310, p. 1553–1594.

Xie, W., 2012, Geological background and genesis of the Late Devonian Heishan magmatic sulfide-bearing intrusion in the Beishan fold belt, NW China: Unpublished Ph.D. thesis, Guiyang, China, Institute of Geochemistry, 137 p. (in Chinese with English abs.).

Xie, W., Song, X., Nie, X., and Cheng, S., 2011, Features of the mantle source and tectonic setting of the Poshi Ni-Cu sulfide-bearing intrusion, Xinjiang, China: Earth Science Frontiers, v. 18, p. 189–200 (in Chinese with English abs.).

Xie, W., Song, X.-Y., Deng, Y.-F., Wang, Y.-S., Ba, D.-H., Zheng, W.-Q., and Li, X.-B., 2012, Geochemistry and petrogenetic implications of a Late Devonian mafic-ultramafic intrusion at the southern margin of the Central Asian orogenic belt: Lithos, v. 144–145, p. 209–230.

Yang, S.-H., and Zhou, M.-F., 2009, Geochemistry of the ~430-Ma Jingbulake mafic-ultramafic intrusion in western Xinjiang, NW China: Implications for subduction related magmatism in the South Tianshan orogenic belt: Lithos, v. 113, p. 259–273.

Zhang, Y.Y., and Guo, Z.J., 2008, Accurate constraint on formation and emplacement age of Hongliuhe ophiolite, boundary region between Xinjiang and Gansu provinces and its tectonic implications: Acta Petrologica Sinica, v. 24, p. 803–809 (in Chinese with English abs.).

Zhang, Z., Mao, J., Chai, F., Yan, S., Chen, B., and Pirajno, F., 2009, Geochemistry of the permian Kalatongke mafic intrusions, northern Xinjiang, northwest China: Implications for the genesis of magmatic Ni-Cu sulfide deposits: Economic Geology, v. 104, p. 185–203.

Zhou, M.-F., Lesher, C.M., Yang, Z., Li, J., and Sun, M., 2004, Geochemistry and petrogenesis of 270 Ma Ni-Cu-(PGE) sulfide-bearing mafic intrusions in the Huangshan district, eastern Xinjiang, northwest China: Implications for the tectonic evolution of the Central Asian orogenic belt: Chemical Geology, v. 209, p. 233–257.

Zhou, T.F., Yuan, F., Zhang, D.Y., Fan, Y., Liu, S., Peng, M.X,, and Zhang, J.D., 2010, Geochronology, tectonic setting and mineralization of granitoids in Jueluotage area, eastern Tianshan, Xinjiang: Acta Petrologica Sinica, v. 26, p. 478–502 (in Chinese with English abs.).